Risks and Ultraviolet Budgets using Earth Observation (RUBEO): Including a non-standard atmosphere and geographic ozone trend differences in risk assessments.

G. Kelfkens
P.N. den Outer
H. Slaper

Laboratory of Radiation Research,
National Institute of Public Health and the Enviroment (RIVM)

USP-2 report 01-33
USP-2 project 4.1/DE-02
ISBN 90 54 11 378 2

October 2001

This report describes a project carried out in the framework of the Users Support Programme (USP-2), under responsibility of the Netherlands Remote Sensing Board (BCRS)

Contents

Abstract

UV-budget maps (the geographical distribution of effective UV at ground level) can be derived from satellite data. These UV-budget maps visualise changes in effective UV caused by ozone depletion and changes in cloud cover and aerosol content. Alterations in UV-budget maps over time give – in combination with dose-effect models for UV-induced effects – insight in the associated risks for human health and the environment. This report describes the results of the RUBEO-project: calculating Risks and Ultraviolet Budgets using Earth Observation (RUBEO). RUBEO aims at a better cloud parameterisation and incorporating temporal and spatial resolution for surface albedo, aerosol content and tropospheric ozone content. The geographical distribution of ozone and UV climatology and trends over Europe are analysed, and a cost-benefit analysis of satellite based UV budget mapping is provided.
The UV-budget mapping can be applied using TOMS and GOME ozone data. A large scale statistical analysis of cloud effects is given comparing ISCCP and TOMS based remote sensing methods with cloud effects derived from ground measurements. Both satellite derived methods correlate well ($r \approx 0.93$) with the ground based analysis. Correction for non-zero albedo, under clear sky conditions, adds maximal 8% to the yearly effective UV-budget. Temporal and spatial differences in aerosol optical thickness and tropospheric ozone content, result in a decrease in effective UV of 3% for every 0.1 increase in aerosol optical thickness, and in a decrease in effective UV of 4% for every 10 DU increase in tropospheric ozone. Stratospheric ozone trends of –1 to –4% per decade observed over Europe correspond to a 0.5 to 4% increase in skin cancer weighted effective UV. The largest trends are seen in the central part of Western Europe.
At present satellite based UV-budget maps form a functional basis for trend analysis and risk assessment. However, satellite data and ground-based observations are both indispensable. Maps for changing UV-budgets and associated skin cancer risks have been used in ‘state of the environment’, reports. Such overviews, regularly published by the Dutch National Institute of Public Health and the Environment (RIVM) and the European Environmental Agency (EPA), support the evaluation and formulation of adequate environmental policies.

Executive Summary

Satellite data enable the construction of the geographical distribution of effective yearly (or monthly) UV at ground-level, the so-called UV-budget maps. These UV-budget maps support the study of geographical and temporal changes of ground level UV related to changes in the atmosphere, like ozone depletion, cloud changes or increasing aerosol content. Maps for the change in effective UV-budgets give, in combination with dose-effect models for UV induced effects like skin cancer or immune suppression, insight in the associated risk for human health and the environment. This report describes the results obtained in the RUBEO-project: calculating Risks and Ultraviolet Budgets using Earth Observation (RUBEO). RUBEO aims at a better cloud description and incorporating temporal and spatial resolution for surface albedo, aerosol content and tropospheric ozone content. Further, RUBEO attempts to estimate the effect of the (expected) recovery of the stratospheric ozone layer on the future geographic changes in UV levels, and associated skin cancer risks. As a first step we evaluate the geographical distribution of ozone trends over Europe. Finally RUBEO makes a cost-benefit analysis of satellite based UV-budget mapping.

Two methods to calculate the reduction of UV-budgets by clouds, based on satellite data (ISCCP and TOMS), are compared with an empirical ground based correction in a large statistical analysis for different locations over Europe. Both, ISCCP and TOMS, give reliable estimates for ground level UV. For practical reasons, mainly data availability, the TOMS method is used in the present RIVM UV budget mapping.

We developed a method to correct the UV-budget maps for non-zero surface albedo. Results for clear sky conditions, indicate a substantial increase (30-40%) in effective UV in the winter months for northern Europe. The effect on yearly effective UV doses is much smaller, maximal 6-8% for north-west Scandinavia.

A correction on the UV-budget maps for temporal and spatial differences in aerosol content was implemented. Such differences result in a decrease in effective UV of about 3% for every increase of 0.1 in aerosol optical thickness. For lack of aerosol data with geographical and temporal resolution, the impact on UV-budget maps could not be evaluated in detail.

We extended the mapping procedure with a correction for ozone in the troposphere. The effective UV decreases with 4% for every 10 DU increase in (tropospheric) ozone. Because we have no information on the geographical and temporal distribution of tropospheric ozone, this effect can not yet be fully included in our UV-budget maps.

Stratospheric ozone content over Europe for the period 1979-1991 has been investigated. On basis of the year average ozone a consistent negative trend is found, ranging from –4% per decade for the central part of north-west Europe to –1% for north Africa and north Scandinavia. Ozone trends based on monthly averages show a much higher variability. A thorough uncertainty analysis must be performed before we can couple these observed trends to the scenarios for stratospheric ozone recovery. The effective UV over Europe shows an upward trend of 0.5 to 4% per decade. The UV trend is largest over central Western Europe.

Satellite data in combination with a UV transfer model make at present a solid basis for the construction of UV-budget maps for Europe. Mainly because of good time and spatial coverage, good separation of ozone effect and good stability and availability of the data. However, ground-based measurements are indispensable as an additional information source.

European maps for changing effective UV-budgets and skin cancer risks form an essential part of national and international state of the environment reports. Such overviews, regularly published by the Dutch National Institute of Public Health and the Environment (RIVM) and the European Environmental Agency(EPA), support the framing and implementation of adequate environmental policies.

1 Introduction

1.1 UV climatology and environmental (risk) assessment

The stratospheric ozone layer shields the earth surface from harmful ultraviolet radiation (UV, electromagnetic wavelength range from 100-400 nm)). The UVC region (wavelengths in between 100 and 280 nm) is virtually entirely absorbed. Ozone absorption in the UVB (wavelength range from 280 nm to 315 nm) is substantial, while absorption in the UVA (UV wavelengths in between 315 nm and 400 nm) is only small. Consequently, the depletion of the stratospheric ozone observed over the last two decades, probably caused by emission of halocarbons, mainly results in higher UVB doses. Increased UVB at ground-level can induce a wide range of harmful effects on human health and the environment. For instance: an increase in skin cancer, cataracts, a decrease in bio-mass production and crop yields, and suppression of the human immune system [United Nations Environmental Program (UNEP), 1998]. To quantify the risks for human health and environment, information on the spectral changes in UV irradiance at the earth surface is needed. A clear anti-correlation between ozone and ground-level UV has been demonstrated [Madronich, 1992; World Meteorological Organisation (WMO), 1995] and an upward trend in clear-sky UV-dose in relation to a downward trend in ozone has been established [Zerefos et. al.,1998; Mckenzie, 1999]. A solid upward trend in yearly UV dose measured on the ground could not be verified, simply because there are no stable long term (spectral) measurements and year to year variations induced by atmospheric conditions (cloud cover, aerosols content) are large. Apart from direct measurements, ground-level UV doses can be derived using remote sensing techniques [Herman et al., 1996, Bordewijk and Van Der Woerd, 1997, Meerkoetter et al., 1997, Krotkov et al., 1998]. These satellite based methods have been validated to yield good estimates for UV doses at ground-level [Herman et al., 1999, Kalliskota et al, 2000, Matthijsen et al., 2000, Slaper et al., 2001]. Thus, satellite data can be used to calculate the geographical distribution of effective UV doses at ground-level, the so-called UV budget maps. The way these UV budget maps changed over the last two decades can, in retrospect, be used to assess health and environmental risks associated with a changing UV climate. In prospect, the pace of recovery of the stratospheric ozone layer will be decisive for the future risks associated with increased UV levels. Restrictions on production and use of halocarbons were internationally established in the framework of the Vienna Convention, and later intensified under the Montreal Protocol (1987) and the Copenhagen Amendment (1992). This ultimately resulted in a scenario where the production of the most potent ozone depleting substances is phased out by 1995. The effect of these restrictive measures on the increase in skin cancer was first calculated by Slaper for a fixed ozone trend for the Northern hemisphere of –3.9% per decade [Slaper et al., 1996]. Our mapping procedure enables us to expand this approach to a geographically resolved assessments of health and environmental risks over Europe, in view of the international policy to counteract ozone depletion.

1.2 Survey of the report

1.2.1 UV budget maps and risk assessment

Use in risk assessment and environmental policy imposes several requirements on the UV budget maps, and on the underlying methods. The main demands are:

- A reliable method to analyse UV changes over a prolonged period of time;
- A way to separate man induced changes from natural variability;
- A method that can account for all relevant atmospheric parameters;
- A method with sufficient spatial resolution;
- A validation of the method against ground based measurements over shorter time periods and for a small number of stations;

The UV program running at the National Institute of Public Health and the Environment (RIVM, Bilthoven) aims at improving and validating the UV mapping procedure with respect to these requirements.

1.2.2 Connection of RUBEO and other projects

This report summarises the results and activities of the project Risks and Ultraviolet Budgets using Earth Observation (RUBEO, project number 4.1/DE-02). The RUBEO project is a continuation of the BCRS-pilot project 'Ultraviolet Dose Maps of Europe' and the BCRS project 'Climatology of Ultraviolet Budgets using Earth Observation' (CUBEO) both carried out at RIVM, Bilthoven. The BCRS-pilot resulted in a method for UV budget maps based on remote sensing data. In the CUBEO project this method has been validated on basis of ground based UV-measurements. The evaluation of clouds effects has been improved and a model for the development of UV-induced skin cancer has been added to the pilot method. Eventually, this led to a pre-operational prototype for the 'Assessment Model for UV Radiation and Risks' (AMOUR). This pilot version of AMOUR works with a quasi stationary surface albedo, atmospheric aerosol content and tropospheric ozone content. The risk assessment in the pilot version can not be linked to emission scenarios for ozone depleting substances.
RUBEO intends to improve the prototype of AMOUR, mainly on these points. We focus on:

- A more extensive validation of cloud effects (with respect to CUBEO);
- Development of a method to include local and temporal variations in ground reflection, aerosol optical properties and concentration of ozone in the troposphere and implementation of this method on our UV mapping;
- Coupling the budget mapping to the RIVM UV-chain-risk model, relating emission scenarios for ozone depleting substances to future skin cancer risks;
- An overview of the benefits of the satellite based approach for risk assessments compared to surface based methods;

The RUBEO project has profited from RIVM participation in several (international) projects and campaigns: the EU-project MAUVE (Mapping UV by Europe), the MAUVE intercomparison campaign at Garmisch-Partenkirchen, and the EU-project EDUCE (a European Database for Ultraviolet radiation Climatology and Evaluation). The BCRS project SULPHATE provided the basis for the implementation of spatial resolution for aerosol content and tropospheric ozone (see 2.6).

1.2.3 Outline of the report

This introductory chapter is preceded by an abstract and an executive summary giving the aims and results of the RUBEO project in a nutshell. Chapter 2, following this introduction, summarises the RIVM methodology to compute UV budget maps and risk maps based on satellite data. A detailed description is given in the CUBEO-report [Slaper et al., 2001], but for the sake of clarity and readability of this RUBEO report, we include a short recapitulation. In chapter 3 we compare two satellite derived methods for cloud parameterisation with the reduction in radiation measured on the ground. Chapter 4 presents an approach to include regional and temporal variation of albedo, aerosol optical properties and concentration of ozone in the troposphere in our methodology. In Chapter 5 we describe the combination of the UV mapping method and the UV source-risk chain model. As a preliminary result geographically resolved ozone trends over Europe are presented. In chapter 6 we evaluate the advantages of the UV budget mapping based on remote sensing data. Chapter 7 summarises the main conclusions of this report.

2 UV mapping approach at RIVM

2.1 Introduction

In this chapter we present the UV mapping method used at RIVM at the start of the RUBEO project. § 2.2 describes the UV-transfer model and standard input parameters. § 2.3 gives the UV dose calculations based on this transfer model. § 2.4 gives the characteristics of the data provided by the Total Ozone Mapping Spectrometer (TOMS), and the corresponding cloud parameterisation. § 2.5 describes the method for UV risk assessment. § 2.6 summarises the validation of the presented model. In § 2.7 we give a preview on the improvements of the UV mapping procedure, mainly concerning temporal and spatial resolution for surface albedo, aerosols and tropospheric ozone.

2.2 UV transfer model and input parameters

Values for effective UV under a cloudless sky have been calculated with the RIVM radiative transfer model UVTRANS, version 5 (den Outer, 1999). UVTRANS uses a two stream algorithm, with a downward and an upward propagating UV-flux. This algorithm saves substantially on computation time and yields sufficient accurate results for our purpose [Slaper et.al., 2001]. Initially the spectral irradiance as a function of wavelength, λ, solar zenith angle, θ, and total ozone column thickness, O_3, is computed, $E(\lambda,\theta,O_3)$. This spectral irradiance is weighted with an action spectrum, $A(\lambda)$. An action spectrum is a set of weighting factors giving the effectivity for UV of a certain wavelength to induce the effect under consideration. Two action spectra are generally used in the UV mapping procedure: the CIE action spectrum for the induction of erythema in human skin developed by McKinlay and Diffey [McKinlay, et. al., 1987] and an action spectrum for carcinogenesis developed by the Skin and Cancer Hospital in Philadelphia and the University Hospital in Utrecht (SCUPh) [De Gruijl, et. al., 1994]. The spectral irradiance is numerically integrated with the $A(\lambda)$ as weigthing factors, to yield the effective UV irradiance as a function of θ and O_3.

$$UV_{eff}(\theta,O_3) = \int E(\lambda,\theta,O_3) \times A(\lambda)\, d\lambda \qquad (2.1)$$

This $UV_{eff}(\theta,O_3)$ is stored in a two dimensional look-up-table giving the cloudless sky effective UV as a function of solar zenith angle and ozone column thickness.
A fixed set of atmospheric parameters and atmospheric profiles is used to calculate look-up-tables. The parameter set, shown in table 2.1, was used in international model comparisons (van Weele et. al, 2000) and describes conditions common at the RIVM-site in Bilthoven, the Netherlands.

Table 2.1 Atmospheric parameters used to calculate the lookup tables.

Parameter	Value	Profile	Source
Ozone min, ozone max Ozone step	60-500 (Du), 10 Du	Ozone	MLS***
Angle min, angle max Angle step	0-90 (degrees) 1 degree	Pressure	MLS***
Aerosol optical thickness	0.28 (at 320nm)*	Temperature	MLS***
Anisotropy factor aerosols	0.7 *	Aerosol	Demerjian et al. 1980
Wavelength dependency aerosol scattering	1/wavelength		
Albedo aerosols	0.95 *		
Pressure	1013 (hPascal)		
Ozone cross section	Bass&Paur 1984		
Elevation	0 (km)		
Surface albedo	0.02**		
SO_2	0 (Du)		

*: height independent; ** wavelength independent; ***MLS –Mid latitude Standard atmosphere

2.3 UV-dose calculations

The look-up table produced by the UV transfer model is the basis for the calculations of the UV-dose. The UV-irradiance at a given date, time and location is computed by interpolation in the look-up table. The actual θ is determined by time, date and location and the actual O_3 at the given date, latitude and longitude is read from the TOMS ozone data file (see § 2.1.1). The effective UV-irradiance is corrected for variation in earth-sun distance and for altitude. Correction for the effects of clouds is optional (see § 2.1.2). Summation over a given length of time yields the effective UV-dose. Basis for the mapping procedure are the daily effective UV-doses, usually condensed by further summation to effective monthly and yearly UV doses at ground-level.

2.4 Remote sensing data from the Total Ozone Mapping Spectrometer (TOMS)

2.4.1 Ozone data

The operational mapping procedure uses daily data for ozone column provided by the NASA TOMS satellite. Before 1994 TOMS version 7/Nimbus 7 data are used. From the year 1996 the data record from the TOMS version 7/Earth-probe is employed. Total ozone column values measured during a daily overpass around local noon, are given in Dobson Units for a 1.25° x 1.0° (latitude x longitude) grid. Missing day-files are filled in with average monthly

files, also provided by TOMS. TOMS produces quite accurate ozone column data, deviating less than 5% from ground-based measurements for ozone column [McPeters et al., 1996].

2.4.2 Reflection data

Apart from data on total ozone column TOMS also provides reflection data (reflectivity R, range from 0-1.) Before 1994 (Nimbus 7) the reflection at 380 nm is reported. From 1996 (Earth probe) the reflection at 360 nm is given. We used the UV reduction factor, derived from this R by Eck [Eck et al., 1995]. On basis of conservation of energy and a low surface albedo the TOMS derived UV reduction factor TOMS-DF is given by:

$$\begin{aligned} &\text{TOMS-DF} = 1 - R && R > 0.5 \\ &\text{TOMS-DF} = 1 - (R - R_s) / (1 - 2 * R_s) && R < 0.5 \end{aligned} \qquad (2.1)$$

R: TOMS reflectivity
R_S: surface albedo (<< 1)

For details on the TOMS derived cloud parameterisation see § 3.2.2.

2.5 UV risk assessment

The UV mapping procedure yields the yearly effective UV dose at a given location. In general, skin cancer incidence is related to the yearly UV-dose and age according to [Slaper,1987]:

$$I = \gamma * (UV)^c * (l)^d \qquad (2.2)$$

With *UV* the yearly UV dose (assumed unaltered during lifetime), *l* the age and γ a constant reflecting the susceptibility of the population for the induction of skin cancer. The exponent *c* - the optical amplification factor – describes the dose dependence of the incidence and the exponent *d* the age dependence.
If we chose De Bilt, the Netherlands (longitude: 5.2 E, latitude: 52.1 N) as reference location we get:

$$I_0 = \gamma * (UV_0)^c * (l)^d \qquad (2.3)$$

With I_0 skin the cancer incidence in the Netherlands associated with yearly dose UV_0, γ reflecting the (genetic) susceptibility and sun seeking behaviour of the Dutch population and *l* reflecting the Dutch age distribution. Over Europe the yearly UV dose depends on the location, roughly increasing going south.
If at a given latitude and longitude for year y_1, the UV dose is $UV(lat, lon, y_1)$, the skin cancer incidence is:

$$I_1(lat, lon, y_1) = I_0 * \left(\frac{UV(lat, lon, y_1)}{UV_0} \right)^c \qquad (2.4)$$

This only holds if the susceptibility of the population for skin cancer, reflected in the constant *γ*, and age distribution is independent of the location. Of course this is only valid as a fist approximation because genetic susceptibility for skin cancer and sun seeking behaviour are substantially different over Europe. If the yearly UV-dose in a (later) year y_2 changes to *UV(lat, lon,* y_2*)* and this dose remains the same during lifetime, the change in incidence is given by:

$$\Delta I = I_2(y_2) - I_1(y_1) = I_0 * \left[\left(\frac{UV(lat,lon,y_2)}{UV_0} \right)^c - \left(\frac{UV(lat,lon,y_1)}{UV_0} \right)^c \right] \qquad (2.5)$$

ΔI is the change in skin cancer incidence (number of extra cases per million inhabitants per year) if the difference in yearly UV-dose (*UV(*y_2*) - UV(*y_1*)*) is prolonged during lifetime.

Epidemiology indicates that three forms of skin cancer are associated with UV exposure: Squamous Cell Carcinoma (SCC), Basal Cell Carcinoma (BCC) and Cutaneous Malignant Melanoma (CMM). The incidence for SCC in humans is quite clearly related to the lifelong (cumulative) UV-dose, and animal experiments unambiguously point out UV as the causative factor in carcinogenesis. For BCC and CMM findings are different. The incidence (for BCC and CMM) is not related to lifelong exposure, but UV seems to act mainly in the early stages of tumour development (at a young age). Moreover, in absence of an animal model for the UV driven induction of BCC and CMM the role for UV as a causative factor is less unambiguous than for SCC. In fact more sophisticated modelling should be used for the induction of BCC and CMM by UV. But these models are at present not available. Therefor we use relation 2.4 as a first approximation to describe induction of BCC and MCC too. As a result the incidence for all three forms of skin cancer can be described by relation (2.4) with different *c*-parameters and different baseline incidences. From the viewpoint of public health not only the cancer incidence but also the mortality (S) – expressed as the fraction of the people who eventually die from the cancer they have attracted – is a valuable parameter. Mortality differs strongly for the three types of skin cancer associated with UV exposure, ranging from 0.3% for BCC to 25% for CMM.
Table 2.2 summarises the parameters used to describe the change in skin cancer incidence and mortality.

Table 2.2 Parameters used in the skin cancer and mortality risk calculations

Type of cancer	I_0 (baseline incidence)	C (dose depence of I_0)	S (mortality associated with I_0)
SCC	160	2.5	0.030
BCC	900	1.4	0.003
CMM	110	0.6	0.250
Total	1170		

I_0 expressed as the incidence per million inhabitants per year for the Dutch population, data from [Slaper et al., 1996]

On basis of these parameters the total change in incidence and mortality (expressed in excess number of cases or excess number of deaths per million per year) are computed by summing over the three type of skin cancer according to:

$$\Delta I = \sum_{i=1}^{3} I_0(i) * \left[\left(\frac{UV(lat,lon,y_2)}{UV_0} \right)^{c_i} - \left(\frac{UV(lat,lon,y_1)}{UV_0} \right)^{c_i} \right] \quad (2.6)$$

$$\Delta S = \sum_{i=1}^{3} S(i) * I_0(i) * \left[\left(\frac{UV(lat,lon,y_2)}{UV_0} \right)^{c_i} - \left(\frac{UV(lat,lon,y_1)}{UV_0} \right)^{c_i} \right] \quad (2.7)$$

2.6 Improving the UV budget mapping

The standard UV mapping procedure treated surface albedo, aerosols and ozone in the troposphere as quasi stationary variables. In the context of the RUBEO project (temporal and spatial) variations in these parameters have been included in the UV mapping procedure. Beforehand surface albedo is expected to have the most substantial effect. Over snow covered areas albedo may range from 0.1 (old snow) to 0.9 (fresh snow). The high amount of reflected radiation over snow covered areas may be interpreted as originating from clouds, resulting in an underestimation of the effective UV dose at ground-level. For the yearly UV dose the effect will be small because the yearly dose is mainly built up by the summer months. In the summer months the surface albedo is small (≈0.02) and albedo variations are negligible. But to get a more accurate description of the UV budgets during the winter period, especially in Northern Europe, a first order correction for the albedo effect is developed (chapter 4). Temporal and spatial resolved surface albedos were extracted from the TOMS data set. This set contains minimal reflection data for Europe, for every month of the year, averaged over 14.5 years.

For aerosols facts are different. The influence is important during the whole year and the resulting change in yearly UV dose is substantial. Increasing aerosol optical thickness from 0 to 1.0 in our model calculations result in a decrease of the yearly UV dose with approximately 25%. To account for this effect we adapted a method, developed by IVM Amsterdam, in the context of the SULPHATE project. This method calculates the sensitivity (S) of effective ultraviolet for the change in a certain atmospheric parameter, aerosol optical thickness and tropospheric ozone content in our case. In the SULPHATE project it has been demonstrated that this S-parameter is mainly dependent on the solar zenith angle and on the total vertical ozone column thickness. In the RIVM standard look-up tables the effective UVB, under standard atmospheric conditions, is tabulated as a function of the solar zenith angle and vertical ozone column thickness (see 2.1). Based on this look-up table, the deviation of the parameter from its value in the standard atmosphere, and the sensitivity S, we can recalculate the effective UV for a non-standard atmosphere. This approach has been incorporated in the mapping procedure. At present we do not have an aerosol data set with adequate spatial and temporal resolution for Europe. Therefor, the effect of aerosol variability on the UV budget maps could not be further evaluated. But in the near future we hope to obtain aerosol data with temporal and spatial resolution to incorporate the aerosol effects on effective UV.

Ozone concentration in the troposphere is elevated mainly during episodes of summer smog, leading directly to health effects and plant damage. But tropospheric ozone also acts as an UV filter reducing the effective UV-dose at ground-level. Although this effect is expected to be small - compared to albedo and aerosol effects - we extended the UV mapping procedure to incorporate a variable concentration of ozone in the troposphere. But, unfortunately, for tropospheric ozone, there is also no comprehensive data set with sufficient spatial and temporal resolution. Therefor, we could not really check the influence of tropospheric ozone on UV budget maps for Europe. However, we will attempt to acquire tropospheric ozone data with good temporal and spatial resolution to assess the resulting change in effective UV.

Alternative satellite data sets

The UV mapping could be improved with a better satellite data set. An alternative for the TOMS version 7 ozone data is given by the total ozone column data from ESA's Global Ozone Monitoring Experiment (GOME). GOME pixels are larger and it takes GOME three days for full global coverage. However, GOME data can be recalculated with the Assimilation Model of the KNMI (AMK) [Levelt et al, 1996] to GOME level 4 assimilated data in the same format as the TOMS files (Dobson units on a 1.25 x 1.0 longitude x latitude grid). The operational UV mapping method can use TOMS as well as (assimilated) GOME data.

To guarantee consistency and continuity of our UV mapping, comparability of the UV-maps computed on basis of GOME and TOMS is essential. A first comparison, in the context of the CUBEO project [Slaper et al, 2001, page 35-36], indicated that GOME and TOMS UV-maps show significant differences. GOME yields an up to 8% higher estimate for the effective yearly UV-dose. A complicating factor is that the difference between GOME and TOMS based UV is not constant, but depends on the latitude and longitude of the location, generally increasing going to the south of Europe.

In view of these differences it is evident that combining GOME and TOMS data for trend analysis is not a straightforward procedure. Therefor, for now we stick to the TOMS-based approach for UV maps and trend analysis.

In the near future a more fundamental comparison between TOMS and GOME UV-maps is necessary. For instance, to check if the improved assimilation model of KNMI (TM3) reduces the observed differences. A good comparability of GOME and TOMS data products becomes increasingly important as we may be able to recalculate the tropospheric ozone content on basis of the GOME stratospheric ozone profiles, a feature not present in the TOMS data.

On the longer run a further improvement of the UV mapping may be based on the Ozone Monitoring Instrument (OMI), to be launched in June 2003. OMI is a contribution to the EOS Aura mission of the Netherlands Agency for Aerospace Programs (NIVR) in collaboration with the Finnish Meteorological Institute (FMI). OMI will produce ozone data with a higher spatial resolution (36 x 48 km) than TOMS and will improve discrimination between stratospheric and tropospheric parameters.

3 Comparison of TOMS and ISCCP cloud parameterisation

3.1 Introduction

The UV budget maps support risk assessments for effects on health and environment caused by a changing UV climate [Slaper et al. 1996, Slaper et al. 1998]. However the satellite-based method differs strongly from the ground-based measurements with respect to spatial and temporal resolution. The UV maps, on the one hand, provide regional differences, but have low temporal and spatial resolution. Ground-based measurements, on the other hand, yield accurate local data with high temporal resolution, but because of the small number of stations and limited period of operation, regional time-resolved averages can not be produced. As a result of the sampling differences in space and time between ground-based stations and satellites discrepancies in the UV budgets may arise. This holds particularly when cloud cover - which is by nature highly variable in space and time – is taken into account. In this chapter we compare the merits of two satellite-based approaches in the assessment of surface UV levels under a cloudy sky. We compare the reduction of daily effective UV doses based on both satellite data sets with the UV reduction computed from global solar radiation measurements on the ground. Global solar radiation data were derived from the network of the World Radiation Data Centre (WRDC). Satellite data were derived from two sources. The International Satellite Cloud Climatology Project (ISCCP), an ensemble of satellites combined to yield a 3 hour global coverage [Rossow et al., 1996] and from the Total Ozone Mapping Spectrometer (TOMS) aboard the Nimbus-7 satellite (one daily overpass around local noon and global coverage). ISCCP data have a good temporal resolution and are produced since 1985. Because the ISCCP-data set is build up from a large number of satellites it may take up to five years before the validated data become available. TOMS data are available since 1979, have low temporal resolution and are almost real time available (within 24 hours). Aims of this comparison are:

- Compare the ISCCP and TOMS based methods with respect to the estimation of the daily effective UV doses on the ground.
- Assess which approach is the most adequate for the computation of UV budget maps for Europe.

3.2 Methods

We compared the effect of clouds on daily UV doses from two independent satellite data sources (ISCCP and TOMS) with ground-based data (WRDC). The comparison extends over data from four summer months (May, June, July, August) over a six years where TOMS and ISCCP data are available (1986, 1988-1992). We restrict ourselves to the summer period to avoid complications due to high surface albedos caused by snow cover.

3.2.1 UV reduction derived from ISCCP-data

ISCCP is a project specially designed to develop a detailed time resolved cloud climatology with a global coverage. The most recent update, the ISCCP-D1 data set, combines the observations of an ensemble of satellites to a 3 hourly global coverage with grid cells of 280 km x 280 km equal-area (2.5˚ latitude x 2.5˚ longitude at the equator, 6596 grid cells in total). Figure 3.1 depicts the European part of this grid. We just give the main characteristics

relevant for this report. Detailed information is found in Rossow et al., 1996. For every ISCCP grid cell the D1 data set contains cloud cover and cloud optical thickness. Measurements are performed at individual pixels within the grid cell, each grid cell containing 60-100 pixels. To yield a valid measurement for an ISCCP grid cell data for at least 20 pixels must be available. Otherwise the grid cell is discarded. Cloud cover (f) is defined as the fraction of cloudy pixels in the grid cell, as seen in the visible and infrared ([Rossow et al., 1993], [Rossow et al., 1996]). Cloud optical thickness (τ_{cld}) is computed by comparing, for every pixel, the measured (reflected) radiance for visible light (600 nm) with calculations based on a radiative transfer model. The optical thickness for the ISCCP grid cell is an average value based on the reflectance for each pixel.
We use f and τ_{cld} to compute the daily mean UV reduction factor, referred tot as the ISCCP-DF (ISCCP derived daily reduction factor). The ISCCP-DF is defined by Spinhirne and Green, 1978:

$$\text{ISCCP-DF} = \frac{\sum\overline{(UV_{cs}\,(1- f * (1-C_T(\tau_{cld},\theta))\,)}}{\sum\overline{UV_{cs}}} \qquad (3.1)$$

UV_{cs} is the clear-sky UV dose and $C_T(\tau_{cld},\theta)$ the instantaneous reduction by clouds, defined as the ratio between the actual UV dose (at cloud optical thickness τ_{cld} and solar zenith angle θ) and the clear-sky UV dose at the same zenith angle. Overbars denote a one-hour average. For the UV reduction function we use the $C_T(\tau_{cld},\theta)$ experimentally determined by Matthijsen. This $C_T(\tau_{cld},\theta)$ function gives a satisfactory accurate description of the clouds effects on UV for low surface albedo and low aerosol burden. For details on the $C_T(\tau_{cld},\theta)$ and the definition of the ISCCP-DF we refer to Matthijsen et al., 2000.
Every day yields one ISCCP-DF daily reduction factor for every grid cell. The period under consideration covers 123 days (the summer period) for 6 years. Thus without drop outs we get 738 (123 days x 6 years) ISCCP-DF reduction factors for each grid cell.

3.2.2 UV reduction derived from TOMS data

An second description of UV reduction by clouds is derived from daily reflectivity data produced by the Total Ozone Mapping Spectrometer (TOMS) aboard the NASA satellite. satellite. For the TOMS derived daily UV reduction factor (TOMS-DF) we use the relationship given in (2.1). Grid cells from ISCCP are about 5 times larger than TOMS grid cells. To make the TOMS data comparable to the ISCCP data we determined which TOMS grid cells overlapped with a particular ISCCP grid cell and the fraction of the TOMS cell lying within this ISCCP grid cell. The TOMS derived UV reduction factor for the ISCCP grid cell is then computed as the weighted average of the UV reduction factors for the individual TOMS grid cells with the overlapping fraction (of the TOMS cell) as weighting factor. We refer to this (averaged) UV reduction factor for the ISCCP grid, based on TOMS data as TOMS-DF (TOMS derived daily reduction factor).

3.2.3 UV reduction derived from Global Solar Radiation

UV reduction factors were derived from routine pyranometer measurements of global solar radiation (all wavelengths in between 0.3 and 2.8 μm). We used data from 125 ground stations linked to the World Radiation Data Centre (WRDC), [WMO, 1987]), see the circles in figure 3.1. The method is described in detail in Matthijsen et al., 2000. In summary: the calculation of the daily UV reduction factor is based on an empirical derived C_F-function. This C_F-function relates the ratio of measured global solar radiation (G_i) and clear-sky global solar radiation ($G_{CS\ i}$) at station i to the daily UV reduction. This ratio of the actual UV daysum and clear-sky UV daysum is referred to as GDF_i. (ground-based daily reduction factor). The ground-based daily reduction factor GDF for the ISCCP grid cell is then defined as the average of the GDF 's for the individual ground stations.

$$GDF = 1/n_S \sum GDF_i = 1/n_S \sum C_{F(}G_i, G_{CS\ i}) \qquad (3.2)$$

n_S : the number of WRDC-stations in the grid cell

Matthijsen used a zenith angle independent C_F function. However, the ratios of direct and scattered radiation for UV and broadband radiation have a different zenith angle dependence [Bodeker , Mckenzie, 1996, den Outer et al. 1999]. Therefore, C_F does in fact depend on solar zenith angle. To account for this effect den Outer introduced a solar zenith angle dependent C_F function. To get a more accurate description of the GDF we used this C_F-function. For a detailed discussion on the zenith angle dependence of the C_F-function see [den Outer et al., 1999]

3.3 Results

We selected 12 representative ISCCP grid cells scattered over Europe with respect to longitude, latitude, and land or combined land/sea cells (see the shaded cells in figure 3.1).

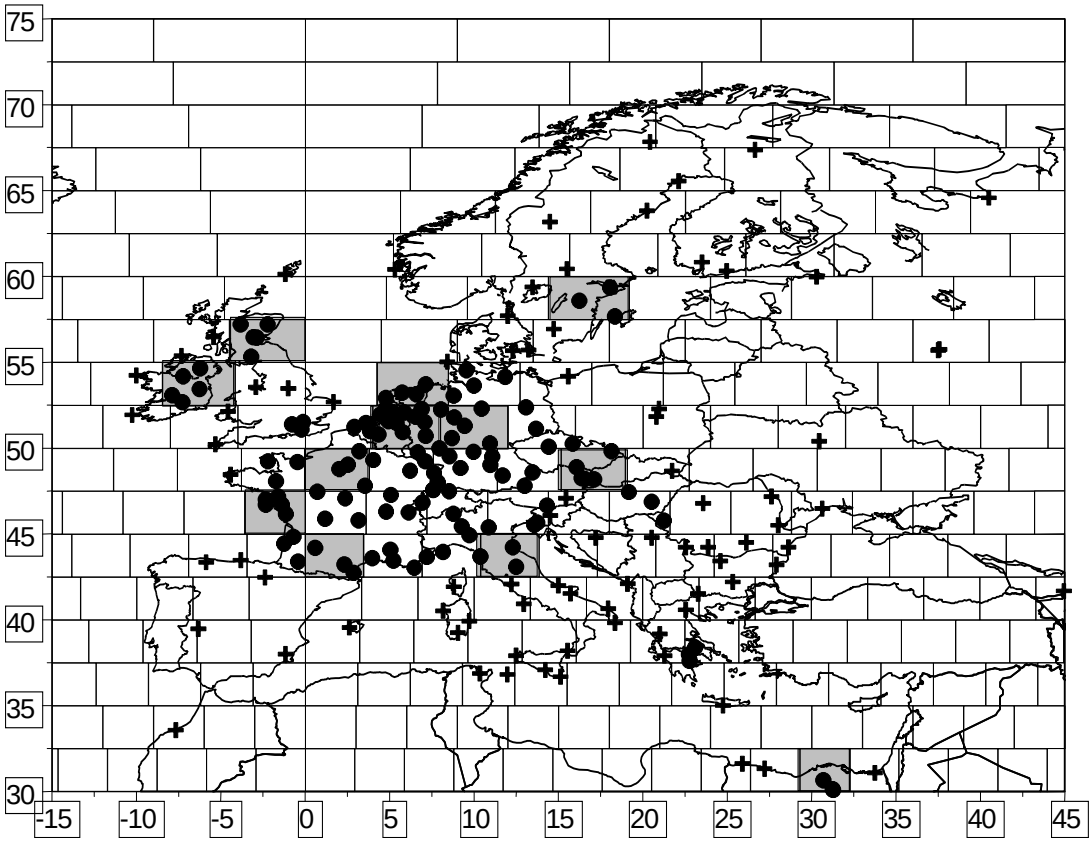

Figure 3.1 280 km equal area ISCCP grid cells. Dots and plusses denote WRDC stations. In this study the dotted stations have been used to supply for data on global solar radiation. The shaded grid cells are the ones used for the comparison of ISCCP-DF and TOMS-DF with ground-based data

For these cells we plotted the relation between ISCCP-DF and GDF and the relation between TOMS-DF and GDF. Figure 3.2 gives the result for three ISCCP grid cells: South France, Belgium + Southern Netherlands and Southern Sweden.

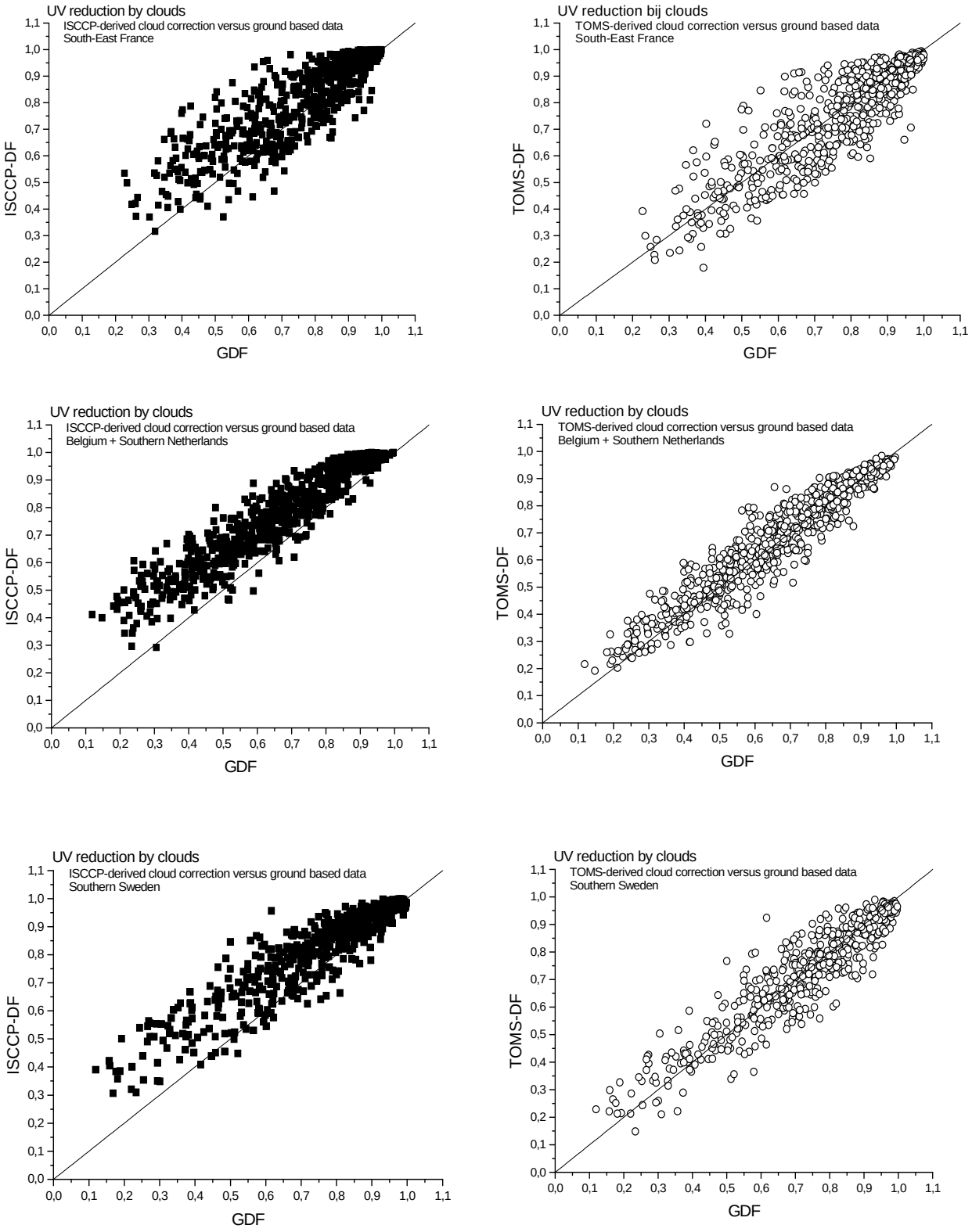

Figure 3.2 Results for the comparison of ISCCP-DF and TOMS-DF for ISCCP grid cells in south-east France, Belgium + Southern Netherlands and Southern Sweden.

Correlation data on all the twelve grid cells are summarised in table 3.1a and 3.1b. Two types of standard deviations are included. The first one is the standard deviation of the satellite data points (y_i) relative to the best linear fit. The second is the standard deviation of the data points relative to the line y=x (TOM-DF or ISCCP-DF = GDF)

Table 3.1 Results for the linear fits of ISCCP-DF and TOMS-DF to the GDF according to: ISCCP-DF = A + B * GDF and TOMS-DF = A + B * GDF.

dA and dB are the standard errors in A and B respectively, R is the correlation coefficient and N the number of valid data points in the grid cell over the evaluated period. For the meaning of the two types of standard deviation see the text.

Table 3.1[a] ISCCP data

Grid cell	ISCCP					
	A ± dA	B ± dB	R	N	SD Best fit	SD y=x
Northern Egypt	0.60 ± 0.02	0.42 ± 0.02	0.64	707	0.03	0.09
South-East France	0.24 ± 0.01	0.75 ± 0.02	0.87	670	0.08	0.10
South-West France	0.32 ± 0.01	0.68 ± 0.01	0.92	677	0.06	0.12
Mid-West France	0.31 ± 0.01	0.70 ± 0.01	0.93	677	0.05	0.11
Northern France	0.26 ± 0.01	0.76 ± 0.01	0.93	667	0.06	0.12
Tsjech rep.	0.27 ± 0.01	0.75 ± 0.01	0.93	736	0.06	0.12
Belgium + Southern Netherlands	0.26 ± 0.01	0.77 ± 0.01	0.94	730	0.06	0.13
Mid Germany	0.26 ± 0.01	0.76 ± 0.01	0.94	702	0.06	0.12
Northern Netherlands	0.37 ± 0.01	0.62 ± 0.01	0.87	731	0.06	0.15
Ireland	0.26 ± 0.01	0.74 ± 0.01	0.91	738	0.06	0.13
Scotland	0.30 ± 0.01	0.69 ± 0.01	0.89	737	0.07	0.15
Southern Sweden	0.27 ± 0.01	0.73 ± 0.01	0.92	548	0.06	0.11
All	0.279 ± 0.003	0.735 ± 0.003	0.918	8320	0.064	0.123

Table 3.1[b] TOMS data

Grid cell	TOMS					
	A ± dA	B ± dB	R	N	SD Best fit	SD y=x
Northern Egypt	0.43 ± 0.02	0.55 ± 0.02	0.70	705	0.03	0.05
South-East France	0.05 ± 0.01	0.92 ± 0.02	0.89	668	0.09	0.09
South-West France	0.14 ± 0.01	0.83 ± 0.01	0.92	676	0.07	0.08
Mid-West France	0.10 ± 0.01	0.86 ± 0.01	0.94	675	0.06	0.07
Northern France	0.02 ± 0.01	0.97 ± 0.01	0.94	675	0.07	0.07
Tsjech rep.	0.02 ± 0.01	0.95 ± 0.01	0.93	738	0.08	0.08
Belgium + Southern Netherlands	0.06 ± 0.01	0.92 ± 0.01	0.95	736	0.06	0.06
Mid Germany	0.03 ± 0.01	0.96 ± 0.01	0.94	705	0.07	0.07
Northern Netherlands	0.16 ± 0.01	0.77 ± 0.01	0.91	730	0.08	0.09
Ireland	0.10 ± 0.01	0.85 ± 0.01	0.90	737	0.07	0.08
Scotland	0.14 ± 0.01	0.82 ± 0.02	0.89	736	0.08	0.09
Southern Sweden	0.08 ± 0.01	0.89 ± 0.01	0.93	548	0.07	0.07
All	0.077 ± 0.003	0.899 ± 0.004	0.929	8329	0.073	0.076

In our computations of the UV budget maps we use the satellite-derived correction factors in combination with the clear-sky UV dose as a direct estimate for the ground-level UV. This approximation becomes more accurate as the (summed) deviation of the satellite-derived reduction factors (TOMS-DF or ISCCP-DF) from the GDF gets lower. Therefor, we included the rightmost column of table 3.1: the summed deviation between the satellite-derived reduction factors and the ground-based reduction factor.
The other 9 grid cells – not shown in figure 3.2 - exhibit the same pattern. Both ISCCP-DF and TOMS-DF are quite well correlated to the GDF factor, the ISCCP-DF being virtually as good as the TOMS-DF. This implies that both ISCCP-DF and TOMS-DF can give a reliable and almost equally accurate estimate for the GDF. A consistent difference, however, is that in the plot TOMS-DF versus GDF the best fitted line almost coincides with the line TOMS-DF = GDF. In the plot of ISCCP-DF versus GDF we see that, although the correlation of ISCCP-DF and GDF is almost equally high compared to TOMS-DF and GDF (see table 3.1), the best fitted line does not coincide with the line ISCCP-DF=GDF. At low cloud transmission the ISCCP-DF overestimates the GDF. This pattern becomes even more evident if we pool all data (figure 3.3).

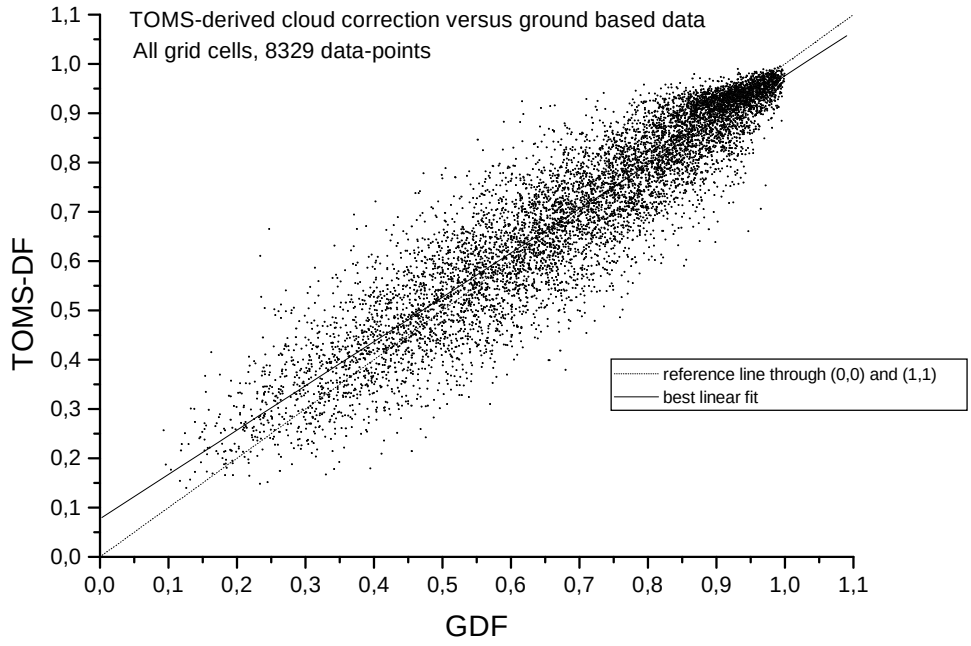

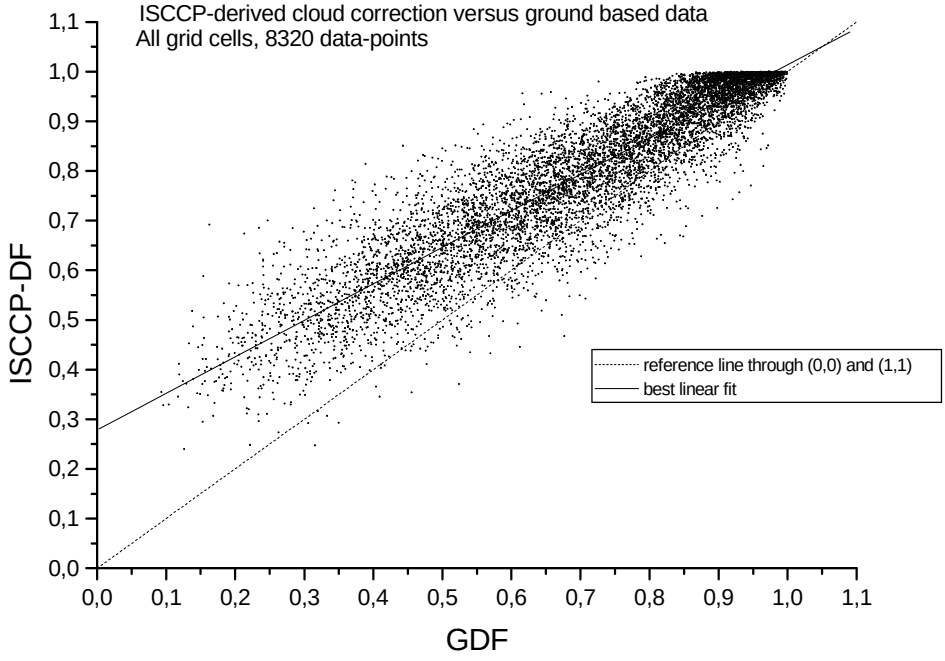

Figure 3.3 Satellite-derived UV reduction factors versus ground-based UV reduction factors; all grid cells taken together.

As our present computations for the UV budget maps are based on the assumption that we may substitute the (unknown) GDF directly by one of the satellite-derived reduction factors without any further correction, the ISCCP-DF is a less accurate estimate for the ground-level UV. As the ISCCP-DF overestimates the GDF the UV budget calculated on basis of the ISCCP-DF will be too high. Although the TOMS-DF performs better it yields a slight overestimation under cloudy skies too.
Table 3.2 gives the amount in which ISCCP-DF (and TOMS-DF) overestimate the GDF and thus the effective UV-dose at the ground-level.

Table 3.2 Percentual difference between GDF and the satellite-based reduction factors ISCCP-DF and TOMS-DF (based on the best fit through the data points, pooled over all locations) over the GDF range. The percentual difference is defined as: 100 * { (ISCCP-DF – GDF) / GDF } (analogous for the TOMS-DF)

GDF	Percentual difference with GDF based on ISCCP-DF	Percentual difference with GDF based on TOMS-DF
0.1	252	67
0.2	113	28
0.3	66	16
0.4	43	9,2
0.5	29	5,3
0.6	19	2,7
0.7	13	0,9
0.8	8,3	-0,5
0.9	4,5	-1,5
1.0	1,4	-2,4

From table 3.2 it is clear that the TOMS-DF yields – in our mapping method - the best estimate for the GDF, and thus for the ground-level UV. The rightmost columns of table 3.1a and 3.1b indicate this also. The standard deviation of the TOMS-DF factor (relative to the function TOMS-DF=GDF) is substantially smaller (0.0758) than the corresponding standard deviation for the ISCCP-DF (0.1233) implying that the TOMS-DF yields a more accurate estimate of the GDF.

Finally we plotted the TOMS-DF versus the ISCCP-DF for all grid cells taken together (figure 3.4).

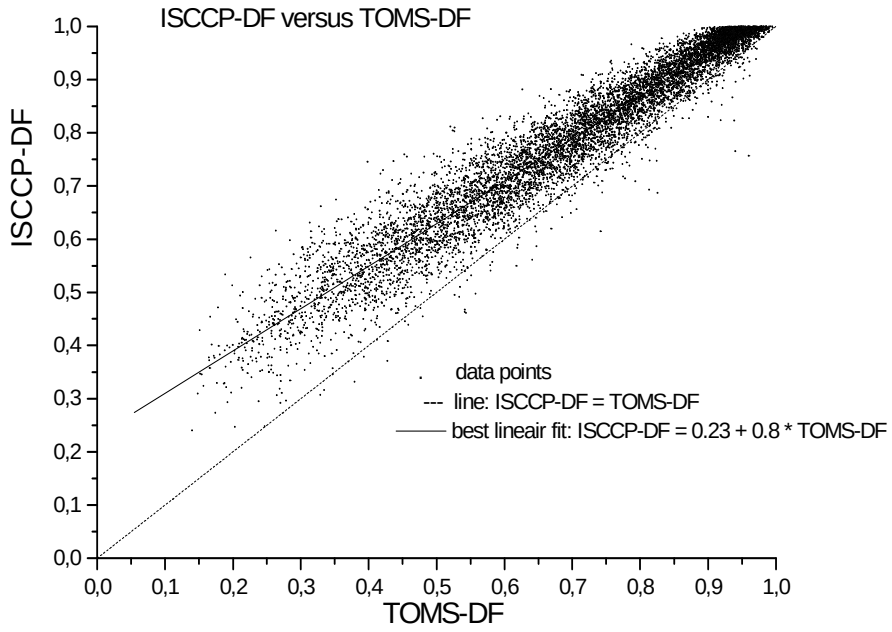

Figure 3.4 Correlation of TOMS-DF and ISCCP-DF, all grid cells together

TOMS-DF and ISCCP-DF are highly correlated, as could be expected on basis of the good individual correlation of TOMS-DF and ISCCP-DF with GDF. The correlation coefficient of TOMS and ISSCP derived reduction factors is R=0.968, pointing to an almost perfect correlation. In accordance with the individual plots of the satellite-derived factors versus the GDF the best fit for the data points does not coincide with the line TOMS-DF = ISCCP-DF, but is shifted to the right and slightly tilted.

3.4 Discussion and Conclusion

Aim of this chapter was to compare two satellite-based methods for the assessment of UV levels on the ground under all weather conditions and to evaluate which of the two methods is most practical in our present computation of UV budget maps for Europe. From figures 3.2 and 3.3 and tables 3.1 it can easily be concluded that both TOMS derived and ISCCP derived factors can be used to give accurate estimates for the GDF. This is a surprising outcome. The ISCCP project - with its high spatial and temporal resolution – is tailored to yield a cloud climatology. As a consequence, we expected this data set to produce the best correlation with the UV budget under cloudy skies. Apparently, the quite rough manner in which the TOMS procedure averages the satellite data over time and space does not lead to a worse correlation with the ground-based data (in fact the correlation is even slightly better) than the more subtle approach – in respect of space and time averaging – of ISCCP. A consistent difference between TOMS-DF and ISCCP-DF is that the TOMS data closely coincide with the line

TOMS-DF=GDF, whereas the best fit through the ISCCP data deviates substantially form the line ISCCP-DF=GDF (figure 3.3). When we use the satellite-derived factors directly, as an estimate for the GDF, without any correction this results in overestimation of the UV budget at ground-level in applying the ISCPP-DF. The TOMS-DF yields a much better estimate of the GDF, but also gives a slight overestimation at low GDF's. The assessment of the GDF could be improved by using the best fits from figure 3.3 (or table 3.1) to calculate the GDF for a given ISCCP-DF (or TOMS-DF). The application of this correction is still under discussion. The omission of this correction may result in a small overestimation of the UV dose at ground level. However, the error in monthly or yearly UV-dose, on basis of TOMS is very small, because overestimation is small and low GDF's are rather seldom.
At the moment we do not have a conclusive explanation why ISCCP overestimates the GDF. A first obvious reason may be a bias in one of the parameters in formula (3.1): cloud cover (f), cloud optical thickness (τ_{cld}) or the function relating cloud optical thickness and zenith angle to the reduction in effective UV ($C_T(\tau_{cld},\theta)$). Calculation of cloud cover is straightforward and a strong bias in this quantity is not expected. Computation of the τ_{cld} is less straightforward. A wide range of atmospheric effects may influence the (computed) value. However, to match the GDF under solid overcast conditions (GDF<0.25) with the $C_T(\tau_{cld},\theta)$ function used by Matthijsen [Matthijssen et al., 2000], the τ_{cld} in the ISCCP D1 data set should at least be underestimated by a factor of two! Such a dramatic underestimation of the τ_{cld} in the current ISCCP analysis seems unlikely. The behaviour of $C_T(\tau_{cld},\theta)$ function itself may give rise to the overestimation of the GDF at low transmission. C_T relates the complex dynamic effects of clouds – defined by just the parameter τ_{cld} measured in the visible region and the zenith angle – to the calculated reduction in effective UV. This makes C_T in principle sensitive to changes in aerosols, ozone, surface albedo and cloud characteristics. This may result in a C_T which drops too slow with increasing τ_{cld} , eventually resulting in too high values for the ISCCP-DF under cloudy conditions. However, the C_T-function presented by Matthijsen [Matthijsen et al., 2000] has been extensively tested under solid overcast conditions, and is relative insensitive to changes in atmospheric conditions. Main influence comes from surface albedo and aerosol optical thickness. In our study surface albedo is practically constant as we only use summer data. Aerosol optical thickness will definitely change substantially over the summer period and over the day. Therefor aerosol concentration may deviate from the average value of 0.4 (at 320 nm) used by Matthijsen, leading to a bias in the C_T -function.
A second explanation for the difference of ISCCP and TOMS may arise from the averaging over the pixels in the ISCCP grid cell. The τ_{cld} for a grid cell is defined as an average value based on the reflectance for each cloudy pixel. In fact, the ISCCP grid cell can be represented as a checker board with a number of squares (at least 20). Some squares are clear, and the others cloudy with different cloud fraction and reflectivity. Averaging the reflectivity over such a checker board to get a τ_{cld} that is representative for the whole grid cell is not a straightforward procedure and may introduce systematic errors.
A third explanation for the discrepancy between ISCCP-DF and TOMS-DF may lie in the characteristics of the radiative transfer models used for calculation of clear-sky values, and/or the different sampling frequencies for TOMS and ISCCP. For instance, the model used by ISCCP neglects the effects of aerosols [Rossow and Schiffer, 1991] but accounts for aerosols near the earth surface by incorporating their effects into the surface properties. This approach results in a high minimum (visible) surface reflectance of approximately 14% over land in summer. TOMS splits up the earth surface reflection and the reflection by a standard

atmosphere resulting in low minimum earth surface (UV) reflectance of about 2% over Europe in summer. The minimum surface reflectance set the dynamic range for the maximum possible reduction by clouds. Differences in the treatment of atmospheric conditions may therefor contribute to the difference between ISCCP-DF and TOMS-DF.
The TOMS data record has some practical advantages as compared to the ISCCP D1 data. The TOMS data are almost real-time available, whereas it may take several years before validated data from ISCCP become at hand. And TOMS data have been available since 1979, 6 years before the ISCCP project started.
In conclusion: Both satellite-based methods investigated are adequate to estimate ground-level UV under cloudy circumstances. In our present UV mapping method the TOMS data set estimates the UV budgets more accurately. For this reason, and because TOMS data are easily accessible we use the TOMS-DF cloud reduction factors for the computation of UV budget maps over Europe under overcast conditions.
Our conclusion regarding the ISCCP data does not - in any respect - alter the fact that this data record it is valuable tool for rendering a reliable, time resolved cloud climatology with global coverage.

4 Implementation of temporal and spatial resolved albedo, aerosols and tropospheric ozone in the UV mapping procedure.

4.1 Introduction

As explained in § 2.6 the accuracy of the UV mapping methodology can be increased by incorporating temporal and spatial variation of surface albedo, aerosol optical thickness and tropospheric ozone into the mapping procedure. In this chapter we give the methods to build these variations into the RIVM UV budget mapping. The approach for incorporating changing albedo effects has been developed at RIVM. The method to account for aerosol and tropospheric ozone effects is an adaptation from the approach developed at IVM in the context of the SULPHATE-project. For all three aspects the adaptations can – in a good approximation - be translated in a more sophisticated calculation of the daily totals for effective UV. This enables us to incorporate temporal and spatial variations into the mapping procedure without changing the overall modeling method. Adaptations made are given in § 4.2 (albedo), § 4.3 (aerosol load) and § 4.4 (tropospheric ozone). For all aspects we use an approximate method, mainly for two reasons. The first reason is that an exact calculation of the effects over Europe would simply cost too much computation time on our computer system. A second reason is that an exact solution is overdone in view of the absence of input data with high spatial and temporal resolution. In each section we further analyze the inaccuracies introduced by using this approximation.

4.2 Effects of variable surface albedo

4.2.1 Background

We evaluate albedo effects on basis of the total transmission of the atmosphere. The fact that total irradiance and effective UV are linearly related to this transmission makes this evaluation valid for effective UV and irradiance too. The ground reflects a fraction of the downward radiation flux back to the atmosphere. This upward flux is partly redirected to the ground (10-40%). As a result, a higher surface albedo yields an increase in total transmission. This effect can be directly verified by calculating the total transmission with the UV transfer model for different surface albedos (see figure 4.1).

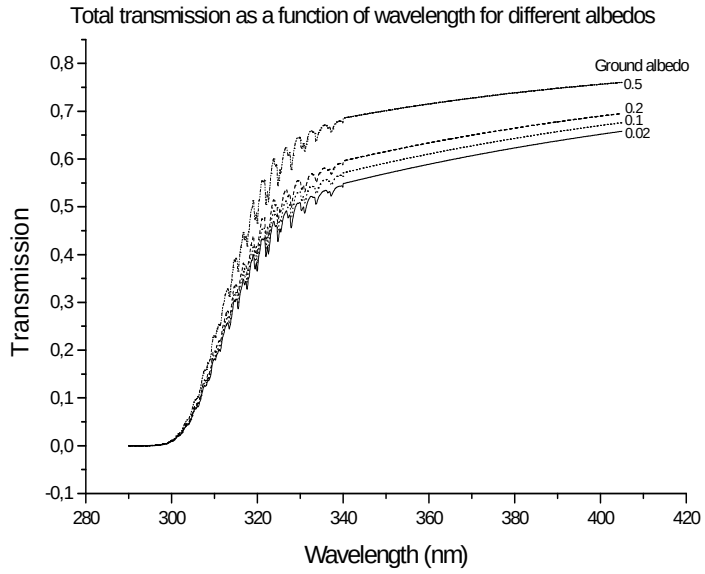

Figure 4.1 Influence of albedo on total transmission at ground-level

4.2.2 General method

We developed a method to incorporate variation in surface albedo in our UV mapping, without having to recalculate the effective UV dose with the transfer model for every (local) albedo. The method is based on the calculation of (infinite) multiple reflections between surface and atmosphere (see figure 4.2). Because of the linearity of the problem and the ground reflection is approximately isotropic, direct and diffuse flux need not be considered separately.

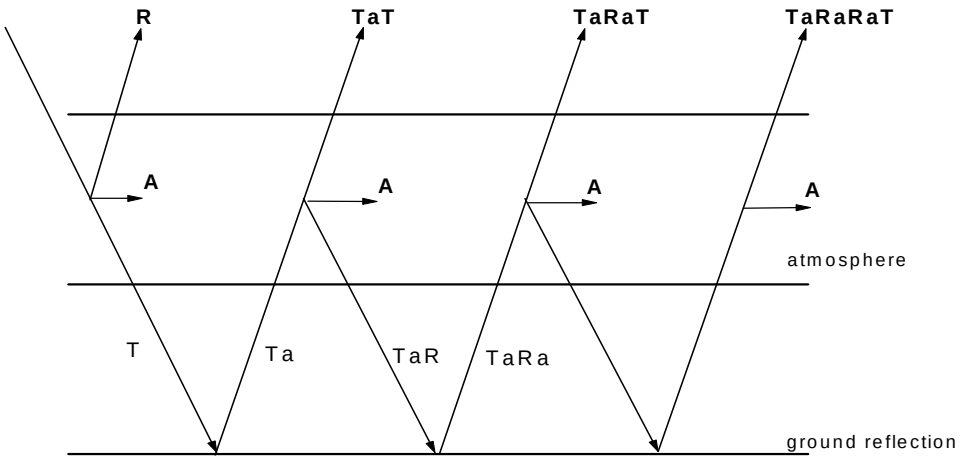

Figure 4.2 Multiple reflections on ground and atmosphere contributing to an increased irradiance at ground-level. R: reflection by the atmosphere, T: transmission by the atmosphere, A absorption by the atmosphere, a: ground reflection

By summing all downward dwelling fluxes, the total transmission at albedo a ($a \neq 0$) is given by:

$$T_a(\lambda) = T_{a=0} + T_{a=0} a R(\lambda) + T_{a=0} a R(\lambda) a R(\lambda) + \ldots\ldots = T_{a=0}/(1 - aR(\lambda)) \qquad (4.1)$$

With $T_{a=0}$ the transmission at a=0, and $R(\lambda)$ the reflection from the atmosphere. T and R are wavelength dependent due to Rayleigh scattering and ozone absorption. $R(\lambda)$ is the quantity to be determined. Inversion of equation 4.1 yields:

$$R(\lambda) = (1 - T_{a=0}/T_a)/a \qquad (4.2)$$

Equation 4.2 enables us to determine the $R(\lambda)$ simply by calculating the transmission for zero albedo and for an albedo $a \neq 0$ with the UV transfer model. This $R(\lambda)$ value yields – via equation 4.1 – the desired transmission or irradiance for a non-zero albedo.

Figure 4.3 gives the ratio for the transmission computed with the UV transfer model and the transmission compute via the method of multiple reflections, for non-zero albedos (equations 4.1 and 4.2).

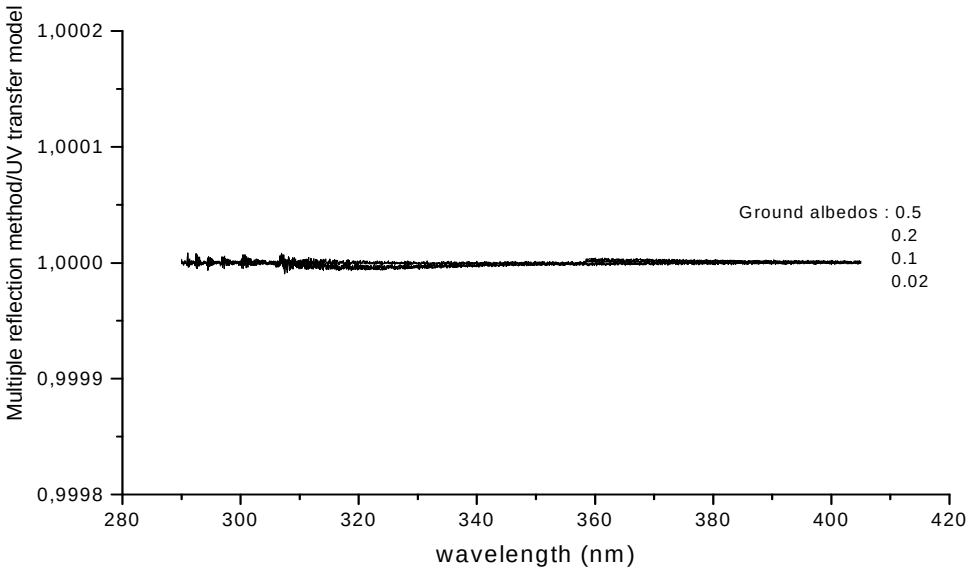

Figure 4.3 Ratio of total transmission calculated with the multiple reflection method and total transmission calculated with the UV transfer model

From figure 4.3 it is obvious that the multiple reflection method is identical to model calculations for non-zero albedos. $R(\lambda)$ depends on aerosol content and slightly on ozone concentration.

4.2.3 Effective R as a function of θ and O_3

In our present mapping approach we first compute look-up-tables with effective UV as a function of solar zenith angle and O_3-concentration. On basis of this look-up-table we compute effective daysums over the year. These daysums are corrected for clouds, height, earth-sun-distance etc. To fit the albedo correction into this procedure we integrate R(λ) over the wavelength range, weighted with an action spectrum, for instance the CIE erythema action spectrum. This yields an effective reflection function for the action spectrum under consideration, denoted as $R_{CIE}(\theta,O_3)$. $R_{CIE}(\theta,O_3)$ depends on zenith angle and ozone concentration. If $R_{CIE}(\theta,O_3)$ depends strongly on θ and O_3, the albedo correction must be done at the level of the look-up-table, before the calculations of the effective daysums. However, a θ and O_3 independent $R_{CIE}(\theta,O_3)$ would imply an albedo correction after the calculation of the daysums, at the same level as the other corrections (clouds, height). This would greatly reduce computation time. We therefor investigated what error is introduced by working with a R_{CIE} independent of solar zenith angle and ozone concentration. Figure 4.6 gives the dependence of R on O_3 concentration, and zenith angle *for an aerosol free atmosphere*. As O_3-concentration range we take 60-500 DU, the standard range for the computations of the look-up-tables.

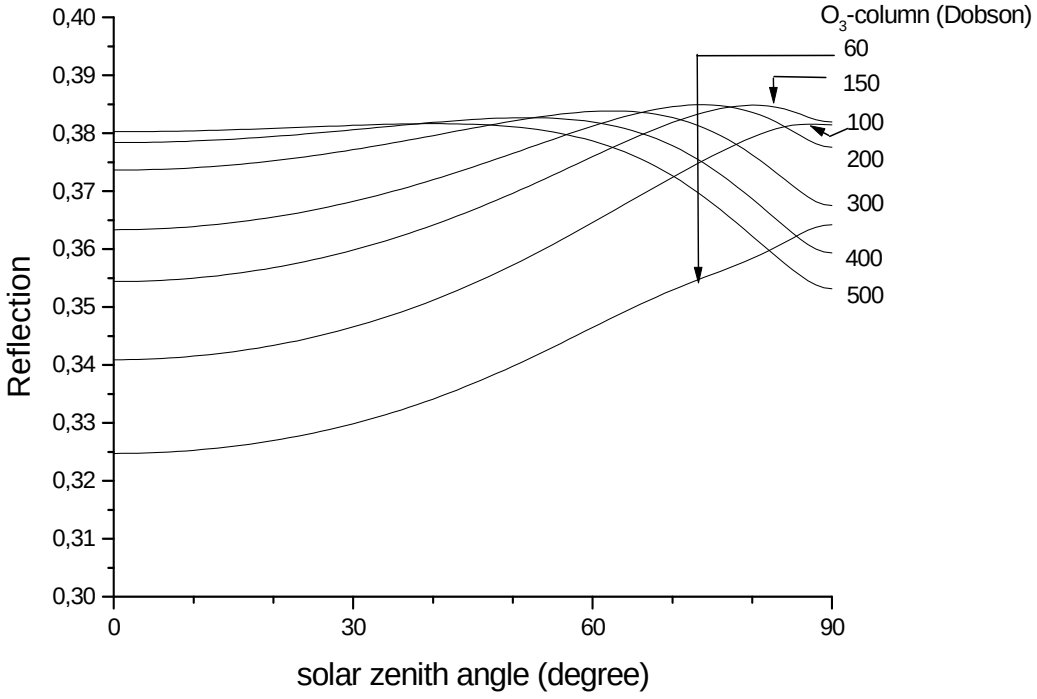

Figure 4.4 Dependence of reflection coefficient R_{CIE} on zenith angle and ozone concentration. Every curve represents the R_{CIE} at a fixed ozone value (60-500 DU). Calculations are for an aerosol free atmosphere.

Averaging the R_{CIE} values over the taken ozone range yields figure 4.5 and averaging R_{CIE} over the zenith angle range yields figure 4.6.

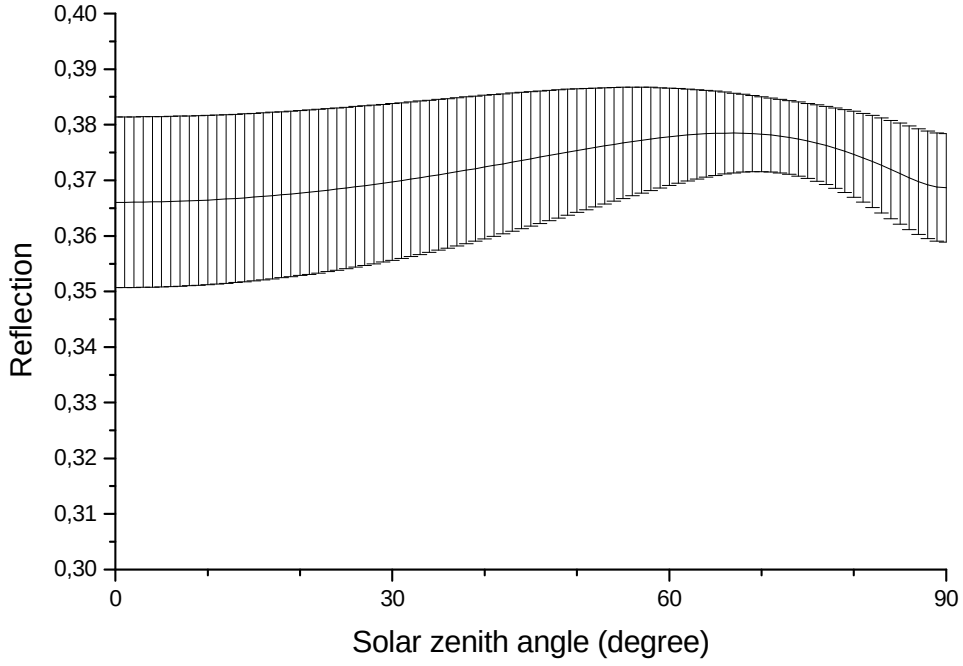

Figure 4.5 Range of reflection values, averaged over the whole ozone range (60-500 DU) as a function of zenith angle for an aerosol free atmosphere.

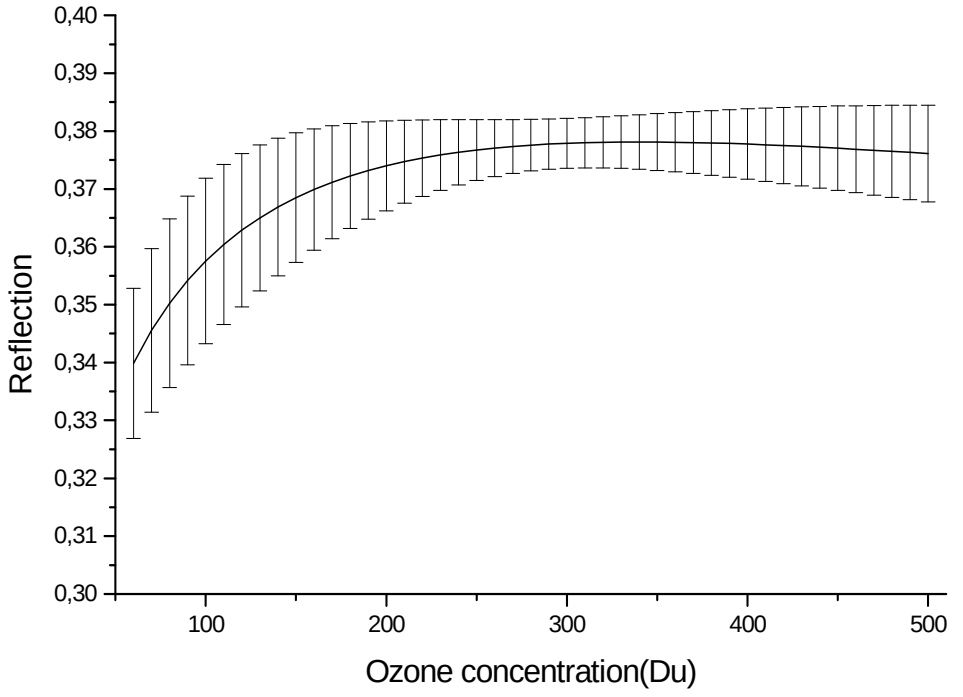

Figure 4.6 Range of reflection values, averaged over the whole zenith angle range (0-90˚) as a function of ozone concentration for an aerosol free atmosphere.

Figure 4.5 shows that R_{CIE} is not strongly dependent on the solar zenith angle (less than 5% variation in R_{CIE} for θ: 0-90˚). R_{CIE} does depend much stronger on the ozone concentration, with variation in R_{CIE} up to 25%. However, if we restrict ourselves to ozone values greater than 200 Dobson units the variation due to changes in ozone reduces substantially to about 5%. This restriction to ozone values above 200 Dobson units is quite reasonable, as ozone values below 200 Dobson units occur quite seldom at moderate geographical latitude. Calculation of the albedo correction factors applying this restriction on ozone concentration results in the curves in figure 4.7.

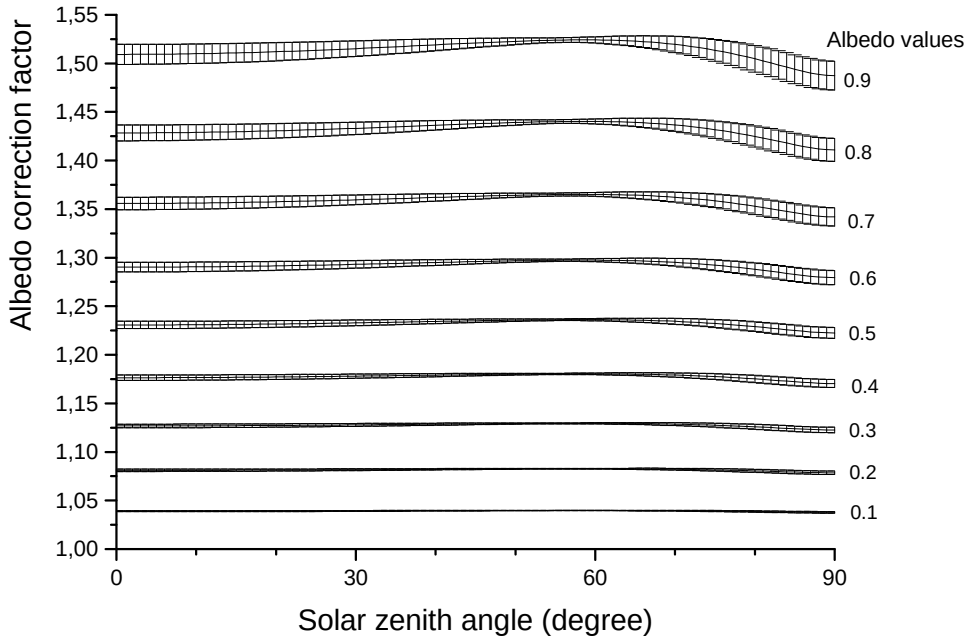

Figure 4.7 Albedo correction factor, averaged over ozone values above 200 DU, as a function of solar zenith angle.

Figure 4.7 makes plausible that the albedo correction factor for ozone values above 200 DU depends only marginally on the solar zenith angle. Especially if we restrict ourselves to zenith angles below 75˚ the variation over the zenith angle range becomes virtually negligible. Table 4.1 gives the mean value for the reflection coefficient R_{CIE} and the standard deviation σ for different θ and O_3 ranges

Table 4.1 Effect of restriction on zenith angle and ozone concentration on (average) R_{CIE} and standard deviation σ.

Restrictions by averaging over θ and O_3	$R_{CIE} \pm \sigma$
No restrictions All θ and O_3	0.372 ± 0.013
All O_3 values $\theta \leq 75^{\circ}$	0.372 ± 0.013
$O_3 \geq 200$ DU All θ values	0.377 ± 0.006
$O_3 \geq 200$ DU $\theta \leq 75^{\circ}$	0.379 ± 0.004

The small variations in the R_{CIE} coefficient as a function of solar zenith angle and ozone concentration justify to calculate a first order correction for the albedo with a zenith angle and ozone concentration independent R_{CIE}. We choose as constant R_{CIE} -value 0.379.

To verify what error is introduced in the effective UV we compared the direct computation with the UV transfer model with the computations based on a fixed R_{CIE} value of 0.379 for different latitudes (see figure 4.8).

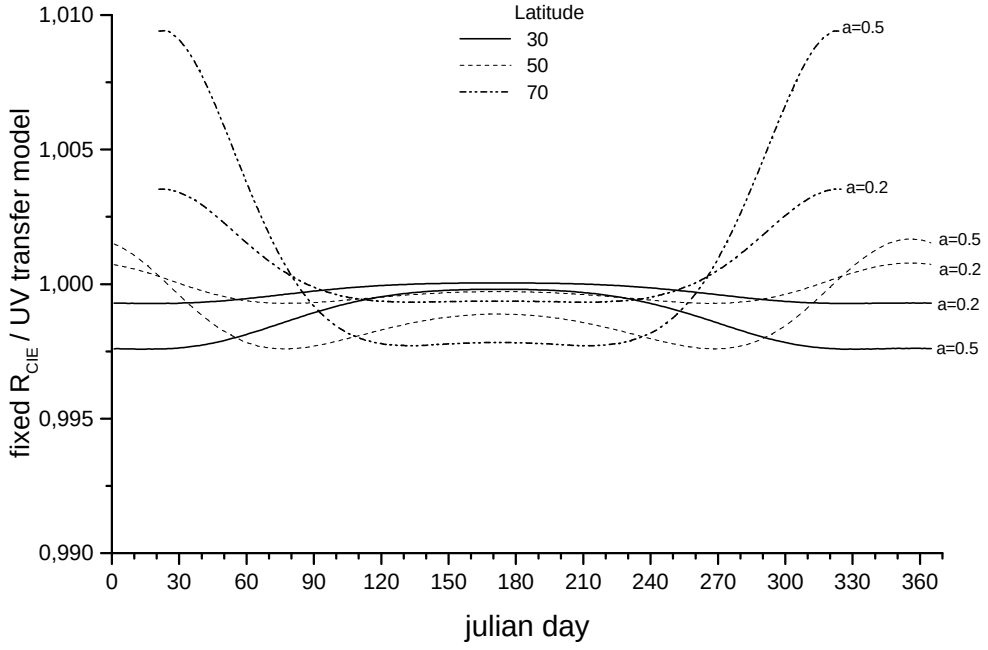

Figure 4.8 Ratio of albedo correction factor calculated with a fixed value of the reflection coefficient (R_{CIE} =0.379) and calculation with the UV transfer model, for latitudes 30°, 50°, 70° and albedo 0.2 and 0.5. Aerosol free atmosphere.

From the figure it is clear that a fixed R_{CIE} -value of 0.379 gives an accurate estimate of the albedo correction. For all days the inaccuracy is less than 1%. If we restrict ourselves to the summer period, which contributes the most to the effective yearly UV dose – the accuracy is even better, about 0.3%.

4.2.4 Aerosol dependence

As a final step we have to include the effect of aerosols on the effective reflection coefficient R. Calculations with the UV transfer model prove that the aerosol dependency can be approximated with a second order polynomial function. Figure 4.9 gives the correction function for the R_{CIE} (for the CIE action spectrum) and under the restriction: $O_3 \geq 200$ DU and $\theta \leq 75^{\circ}$.

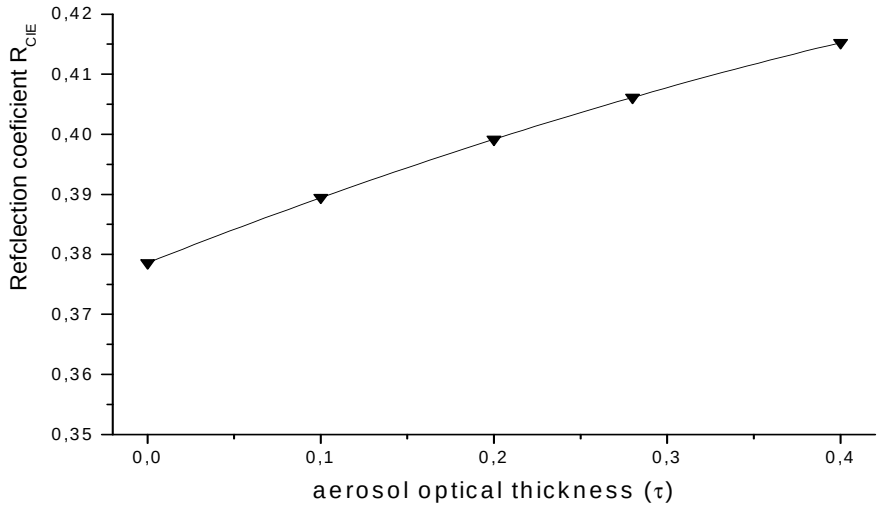

Figure 4.9 Reflection coefficient R_{CIE} as a function of aerosol optical thickness, zenith angle ranging from 0-75˚ and ozone concentration ≥ 200 DU.

Figure 4.9 shows that the aerosol dependency of R can be approximated by a second order polynomial fit. The best fit is given by:

$$R_{CIE}(\tau) = 0.379 + 0.114 * \tau - 0.056 * \tau^2 \qquad (4.3)$$

4.2.5 Conclusion on the method for clear sky albedo correction

To account for albedo variation in the (effective) UV budget mapping we incorporate an effective UV reflection factor R_{CIE} which – in good approximation – only depends on the aerosol optical thickness according to equation 4.3 for the CIE action spectrum. For any other action spectrum the relationship 4.3 has to be recalculated, but we expect similar results. This R_{CIE} can be used for any albedo at a given day and location to compute the albedo correction factor $1/(1-a\ R_{CIE})$. The effective UV at albedo=a can be calculated simply by multiplying the (computed) effective UV at albedo=0 by this albedo correction factor.

4.2.6 Albedo correction for cloudy sky

The presence of clouds will enhance the albedo effect calculated in § 4.2.2, since it increases downward reflection. Therefor, the contribution of clouds to the increase in ground-level UV can be treated similarly as the reflection from the atmosphere. Via the multiple reflection approach we can calculate the albedo correction on the transmission T at albedo=0. The total transmission is now given by:

$$T_a(\lambda) = T_{a=0}(\lambda) * \frac{T_{cld}}{1-a*R_{(cld+atm)}} = T_{a=0}(\lambda) * \frac{1-R_{cld}}{1-a*R_{(cld+atm)}} \quad (4.4)$$

$$R_{cld+atm} = \frac{R(\lambda)+R_{cld}-2*R(\lambda)*R_{cld}}{1-a*R(\lambda)*R_{cld}} \quad (4.5)$$

$T_a(\lambda)$: total transmission, a: surface albedo, $T_{a=0}(\lambda)$: total transmission for albedo=0, T_{cld}: cloud transmission, $R_{(cld+atm)}$: combined reflection of clouds and atmosphere, $R(\lambda)$: reflection of the atmosphere

The (internal) TOMS reflection calculations are corrected for a standard atmosphere. What remains is the combined reflection of the ground and the clouds. Hence the reflection from the clouds can be inferred from the given TOMS reflection by:

$$R_{TOMS} = \frac{a+R_{cld}-2*a*R_{cld}}{1-a*R_{cld}} \Rightarrow R_{cld} = \frac{R_{TOMS}-a}{1+a*R_{TOMS}-2*a} \quad (4.6)$$

This solves the problem to calculate effective UV when at a certain location and time point R_{TOMS} and the local surface albedo are known. R_{TOMS} and albedo give, via equation 4.6 the R_{cld} . Then equation 4.5 with known R_{cld} and $R(\lambda)$ yields the $R_{(cld+atm)}$ (for $R(\lambda)$ see § 4.2.2). Then the right hand size of equation 4.4 gives, with the calculated $T_{a=0}(\lambda)$, the total transmission at albedo a and at the observed TOMS reflection.
Figure 4.9 gives shows the change in he ratio $T_a/T_{a=0}$ as a function of TOMS reflection and the surface albedo.

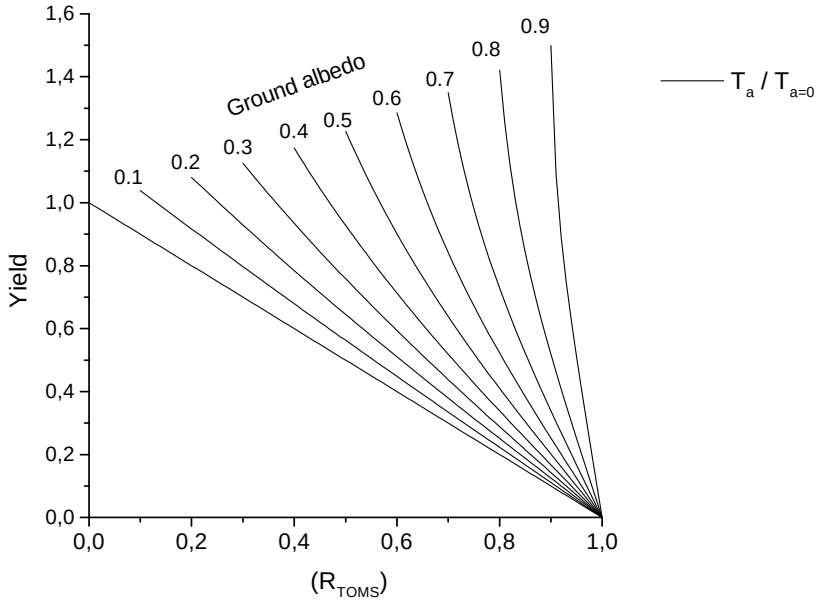

Figure 4.9 Yield, defined as $T_a/T_{a=0}$ (R_{TOMS}; a), under cloudy sky.

Note the reduced range of R_{TOMS} values for non-zero albedo a. The minimal TOMS reflection value is R_{TOMS}=a. The yield value ($T_a/T_{a=0}$) at this TOMS reflection values gives the clear sky albedo correction (§ 4.1).

4.2.7 Validation of the method on basis of the MAUVE campaign

Validation of the albedo correction is difficult because we need data on effective UV over an area with high surface albedo. A first test can be derived form the MAUVE measurement campaign at Garmisch-Partenkirchen in March 1999. At that time the mountains around Garmisch-Partenkirchen were snow covered, although the lower areas and the valleys were green. The minimum reflectivity, measured for the period of the campaign (TOMS overpass data), for the grid cell containing Garmisch was 0.2. Figure 4.10 gives the measured effective UV data from IFU, the albedo corrected model values for a=0.2, and as a comparison the effective UV model values for albedos a=0 and a=0.4

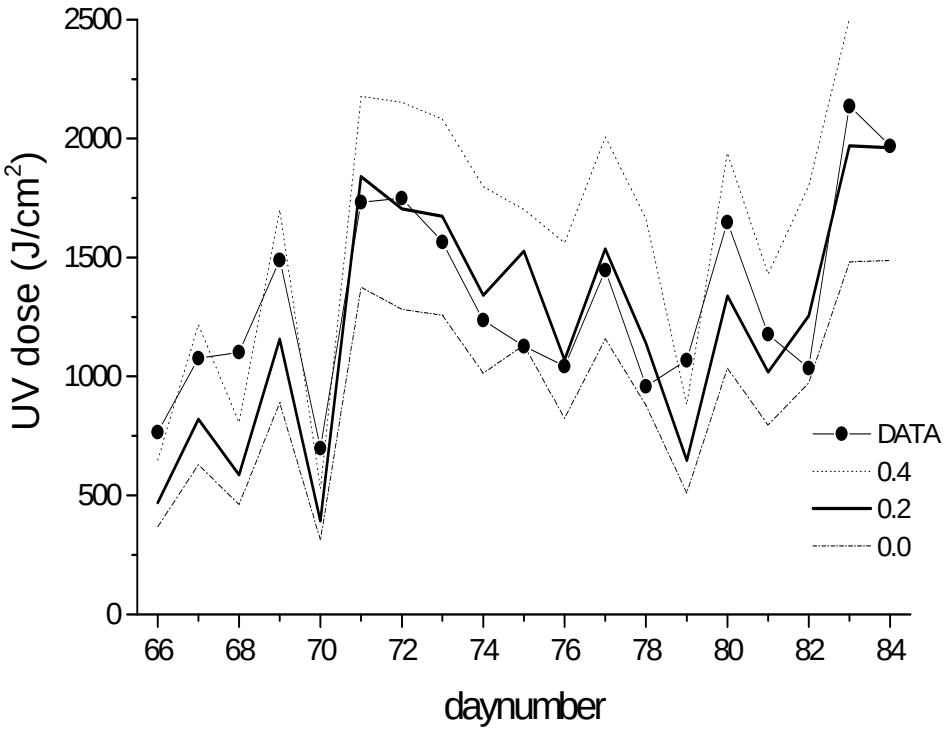

Figure 4.10 Comparison of measured values for the effective UV dose during the MAUVE campaign with the data calculated with albedo correction (drawn line). Calculated data for albedo=0, 0.2 and 0.4 are included.

From the figure it is evident that the measured data are described substantially better with an albedo correction for a=0.2 than in our original modelling (albedo negligible). At the same time we see that we cannot account for the full dynamics of the albedo effects on the UV-dose. This is probably due to the fact that we compare one local measurement with the average minimal reflection for a grid cell covering snowy mountain slopes, but also green pastures. Additional, the effect of clouds, or of a change in surface albedo due to fresh snow may contribute to this discrepancy.

4.2.8 Availability of time and space resolved albedo data for Europe

Albedo data for Europe with a high spatial and temporal resolution are scarce. A comprehensive data set which yields temporal and spatial resolved albedo values is formed by the minimal reflection data computed by NASA on basis of the TOMS/Nimbus7 data files. The data record gives the lowest value for the Lambertian equivalent reflectivity measured over the entire TOMS data record for the period November1978 to May 1993. This Lambertian reflectivity is equivalent to the surface albedo [see Herman and Celarier, 1997]. The spatial resolution of this data set is adequate for our purposes. The temporal resolution, however, is limited, yielding only one albedo value for every month. However, at present this is no other data record. Therefor, we use the TOMS data to estimate albedo effects under clear sky conditions. Figures 4.10 and 4.11 give the minimum reflectivity values for Europe during February (most extensive snow cover) and during July (minimal snow cover).

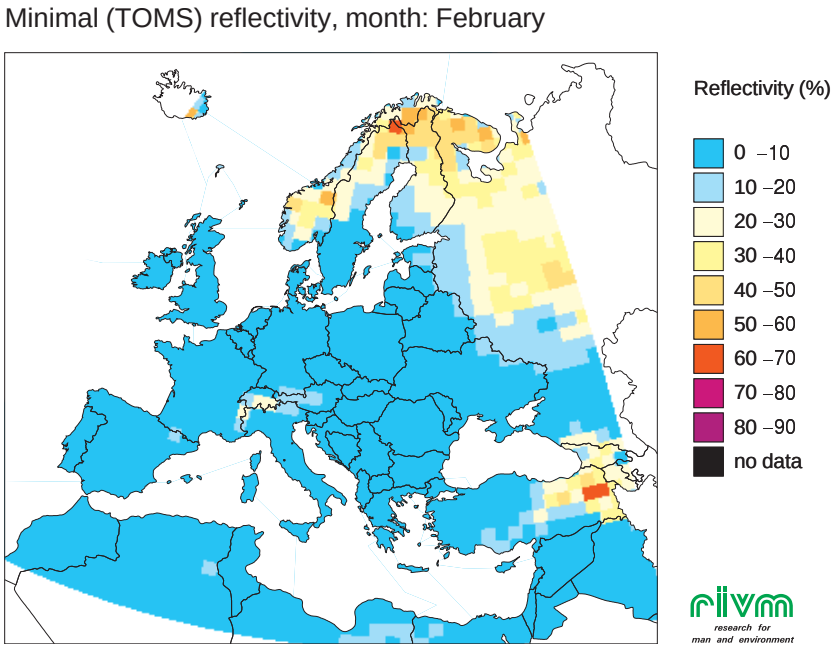

Figure 4.10 Average Lambertian equivalent minimum reflectivity based on the TOMS data record for the month of February.

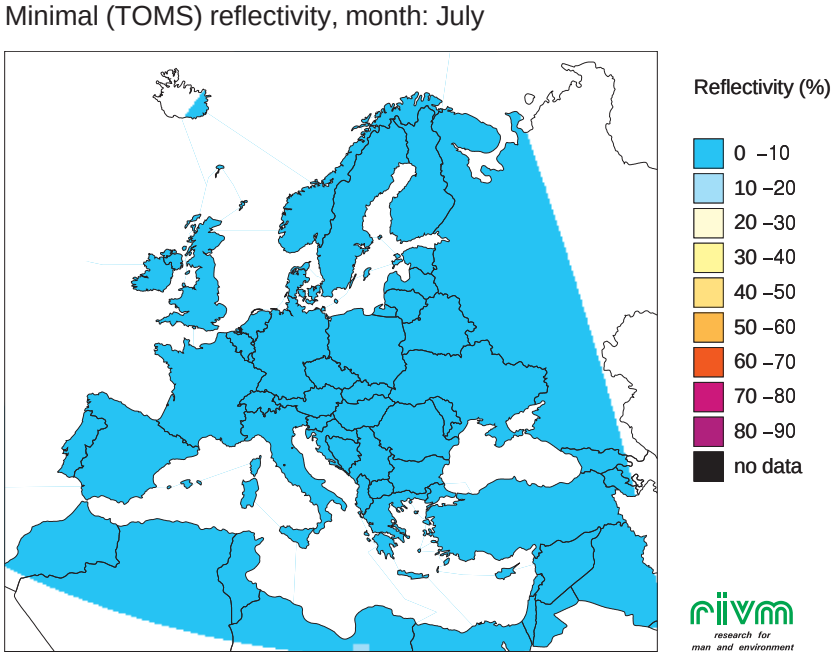

Figure 4.11 Average Lambertian equivalent minimum reflectivity based on the TOMS data record for the month of July

The reflectivity maps confirm that albedo is primarily of importance during the winter months in Northern Europe and over high, snow covered mountains like the Alps and The

Caucasus. With the maximum reflectivity (under clear-sky conditions) reaching up to 68%. During summer the reflectivity over Europe is low, typically around 2%, with a maximum up to 8% in Scandinavia and over the Alps and the Caucasus.

4.2.9 Albedo correction maps

On basis of the TOMS minimal reflection maps we can compute albedo correction factors over Europe for clear sky, using equation 4.1 and 4.3. Results are given for the months of February (figure 4.12) and July (figure 4.13).

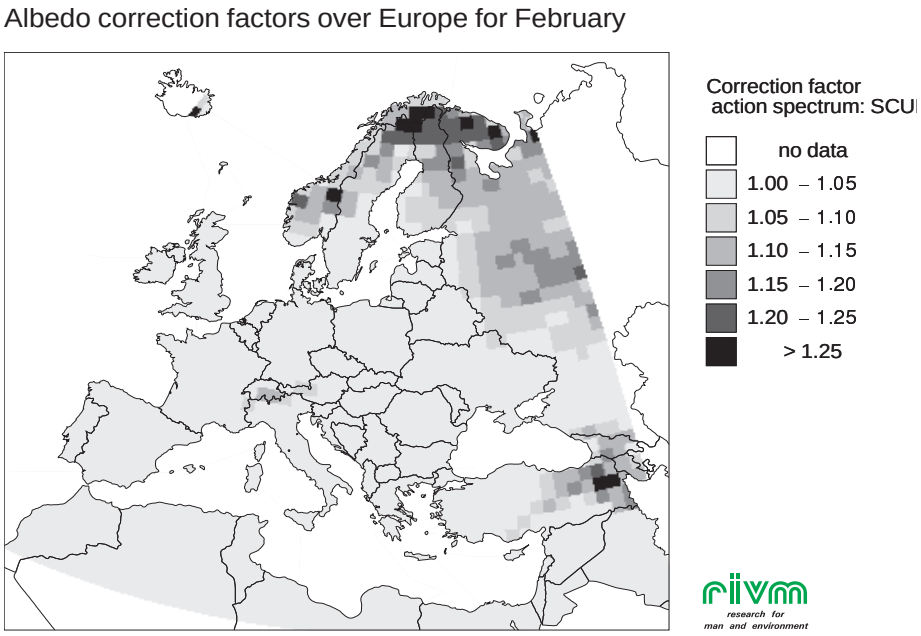

Figure 4.12 Clear sky albedo correction factors over Europe – based on TOMS Lambertian reflectivity - for the month of February.

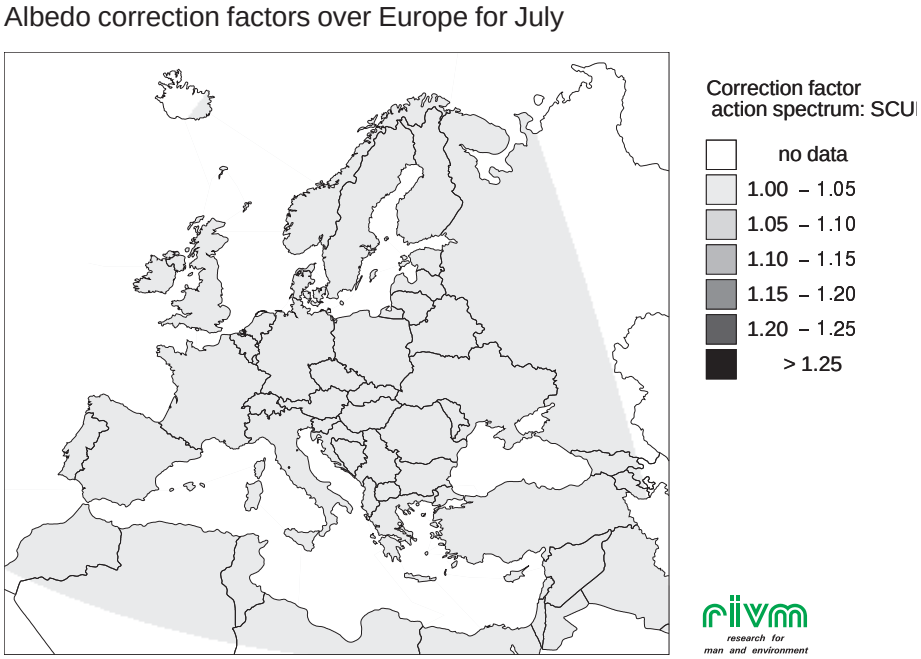

Figure 4.13 Clear sky albedo correction factors over Europe – based on TOMS Lambertian reflectivity - for the month of July.

To correct the effective monthly UV dose for non-zero albedo, we have to multiply the UV dose with the albedo correction factor for the grid cell. From the figures it is clear that (clear sky) albedo correction is important for the February dose, but will have no influence for the doses during the summer month. Because the summer months contribute the strongest to the yearly UV dose the albedo correction only has a small effect on the budget maps for the yearly effective UV under clear sky conditions. If we calculate – for every grid cell - the yearly albedo correction factor by summing the albedo corrected monthly UV doses over the year and calculate the increase of this yearly clear sky UV dose in terms of percentage, relative to the yearly clear sky dose without albedo correction we get the map in figure 4.14.

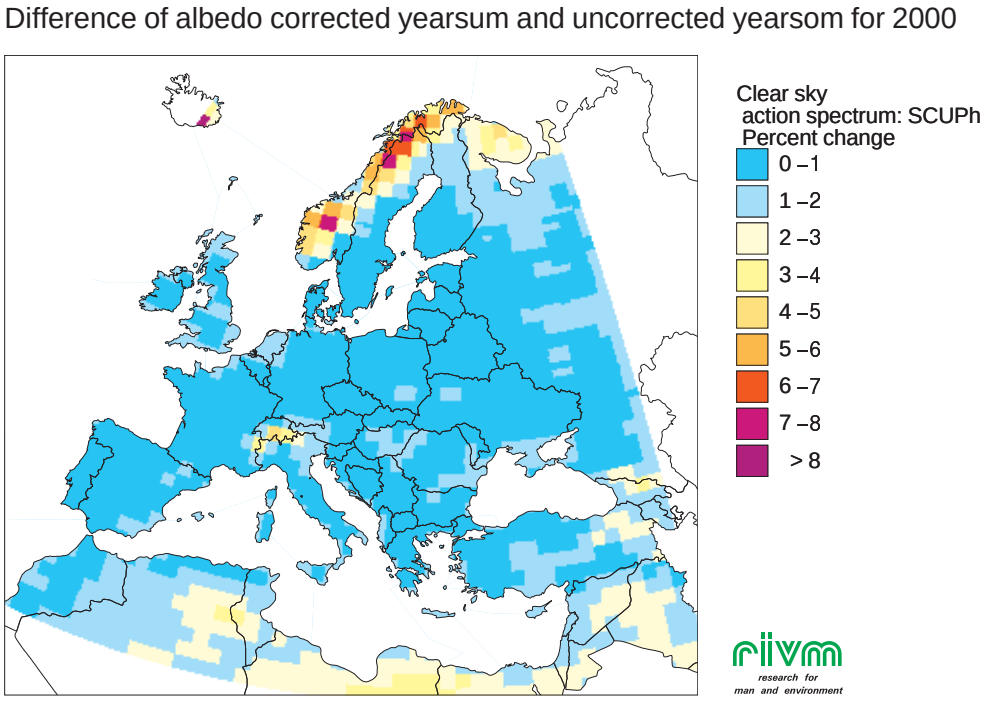

Figure 4.14 Relative increase in effective UV for the year 2000 with clear sky albedo correction, compared to the yearly dose without albedo correction.

From this map it is evident that for most of Europe clear sky albedo correction (relative to albedo=0) is small, typically 0-2%. Over the Alps and over the Caucasus albedo correction may result in an increase in effective UV dose up to 6%. Over the north-west part of the Norwegian mountains we underestimate the effective yearly UV dose – without albedo correction – by 8% at most. Finally there is one ‘white spot’ over the Vatnajökull-glacier in Iceland where the yearly UV dose with albedo correction is almost 18% higher.

4.2.10 Conclusions on albedo influence

In this section we have presented a simplified, but adequate method to correct for temporal and spatial albedo variations. Clear sky correction has been implemented in our UV mapping. A first validation of effective UV doses on the ground yields a reasonable similarity, although further validation of the albedo correction using ground based UV-data sets is required. The albedo correction maps point to substantial corrections (30-40%) on effective UV during winter periods in Northern Europe. During summer the correction is small (about 2% compared with albedo=0). Influence on yearly effective clear sky UV budget is small (maximum 18% in Island, maximum 8% in north west Scandinavia and maximum 6% over high, snow covered mountains). Under cloudy circumstances correction for non-zero surface albedo can be much higher (50-100%). This albedo correction for cloudy situations will soon be implemented in our UV budget mapping.

4.3 Effects of variable aerosol loads

4.3.1 Introduction

In the context of the SULPHATE project a method has been developed at IVM (Amsterdam) to include different concentrations of aerosols in the troposphere in the UV-transfer model (see 2.6). This method calculates the sensitivity (S) of effective ultraviolet for the change in aerosol concentration. The S-parameter is mainly dependent on the solar zenith angle and on the total vertical ozone column thickness. Based on the look-up table for effective UV (see 2.1), the difference of the actual local aerosol concentration and the aerosol concentration in the standard atmosphere, and the S-parameter, the effective UV can be calculated. The IVM-method cannot be implemented right away in the UV budget mapping procedure, because the present UV mapping is based on daysums for effective UV. We developed a method based on the sensitivity parameter S (defined in analogy to IVM) which yields sufficient accurate estimates for the effective UV daysums as a function of aerosol optical thickness (τ).
The sensitivity parameter S is defined by computing effective daysums (UV_0 and UV_1) for every day of the year, for two different values of the optical thickness (τ_0 and τ_1).

$$S(day) = \frac{\ln(UV_0) - \ln(UV_1)}{\tau_1 - \tau_0} \qquad (4.7)$$

On basis of this S(day) we estimate the effective daysum at optical thickness, τ, ($UV(\tau)$) with the formula:

$$UV(\tau) = UV_0 * \exp\left((\tau_0 - \tau) * S(day) \right) \qquad (4.8)$$

To check the accuracy of the S-based estimates we compute effective UV daysums for optical thickness ranging from $\tau = 0.0 – 1.0$. For these calculations we used the UV transfer model to estimate the effective UV daysums under clear-sky conditions.

4.3.2 Dependence of S on string points and daysum

The S parameter is depends on the choice for the two fixed values τ_0 and τ_1, the so-called string points. The dependence of S on the string points is given in figure 4.15.

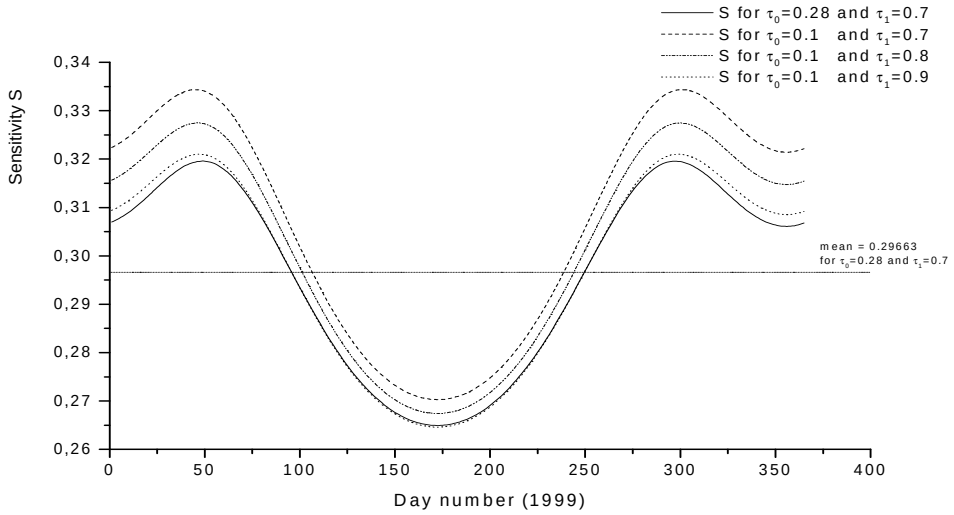

Figure 4.15 Dependence of the sensitivity parameter S defined in equations 4.7 on the choice of the string points. S is plotted as a function of daynumber. Location: De Bilt, ozone column 330 nm.

The average S over the year for τ_0=0.28 and τ_1=0.7 amounts to 0.30, corresponding to a decrease of approximately 3% in effective UV for every 0.1 increase in optical thickness. The choice of the string point affects the sensitivity parameter S and therefor the accuracy of the estimates for the effective UV. To check this effect the percent difference between UV daysums estimated on basis of the S-parameter an computed directly with the UV transfer model is plotted in figure 4.16.

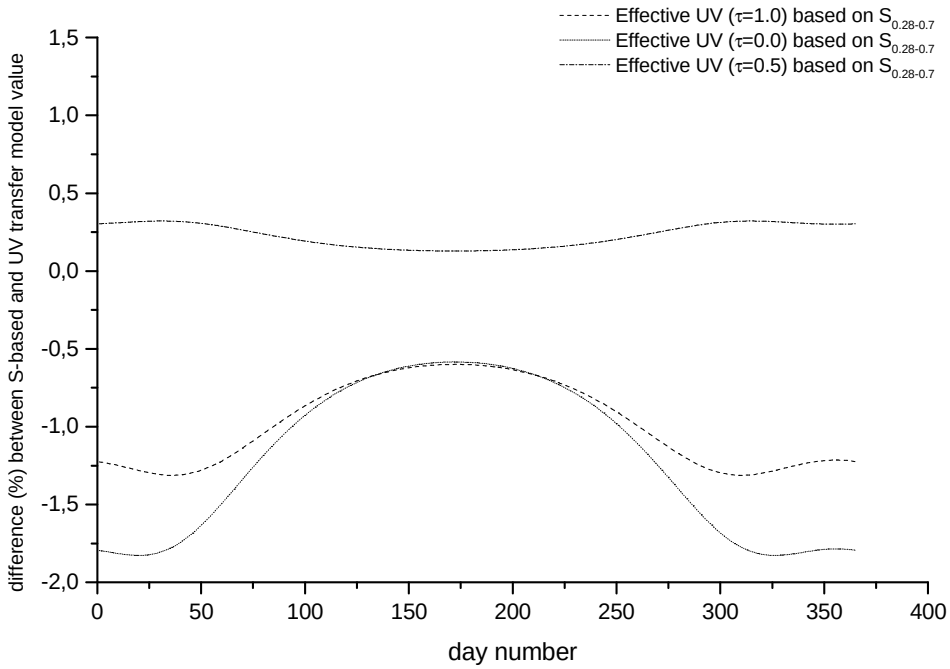

Figure 4.16 Difference in effective UV based on S over the whole τ -range for string points at τ_0=0.28 and τ_1=0.7. Location: De Bilt, ozone column 330 nm.

String points close together give accurate estimates in between the points but relatively poor estimates at both ends of the optical thickness range. The string points τ_0=0.1and τ_1=0.8 give the best overall results. Estimates for the effective UV daysums are within ± 1%of the model values, which is quite acceptable for our purpose (see figure 4.17).

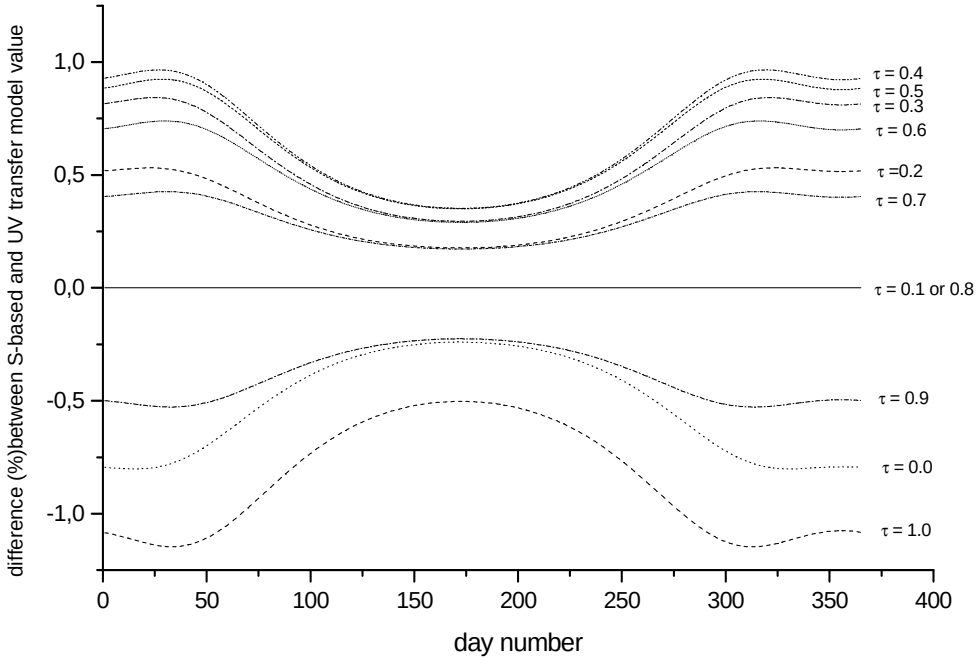

Figure 4.17 Difference in effective UV based on S over the whole τ -range for string points at τ_0=0.28 and τ_1=0.7. Location: De Bilt, ozone column 330 nm.

This S-parameter, determined for De Bilt, ozone column of 330 DU is referred tot as: S(330, De Bilt)$_{0.1\text{-}0.8}$. The S parameter is dependent on the day. Calculations for the UV budgets would be greatly simplified by a day independent S parameter. However, introducing a day independent S substantially increased the difference between the S-based effective UV and the model calculations (deviations from – 4 to +1.5%). We judge this inaccuracy too high for our goal. As a consequence our aerosol correction is based on a day dependent S factor.

4.3.3 Dependence of S on ozone column

In principle S (defined by equation 4.7) depends on the stratospheric ozone content. To check this ozone dependency we computed the S for stratospheric ozone values 230, 330 and 430 DU. (see figure 4.18).

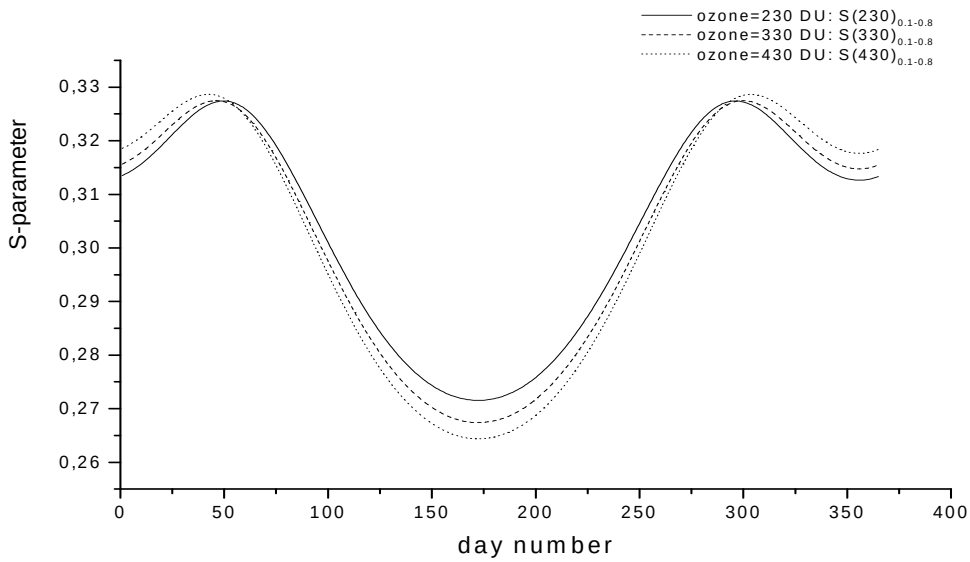

Figure 4.18 Dependence of the S-parameter on ozone column thickness. Location De Bilt, ozone columns of 230, 330 and 430 DU.

The S-parameter does not depend strongly on the ozone column. This implies that the S-based effective UV is not strongly affected by ozone concentration. So we can base our calculations on the $S(330, \text{De Bilt})_{0.1\text{-}0.8}$. To show that this is a valid approximation we plotted in figures 4.19 and 4.20 the difference between the S(330)-based effective UV and effective UV calculated with the UV transfer model for τ =0.0 and τ =1.0 and for 230, 330 and 430 DU.

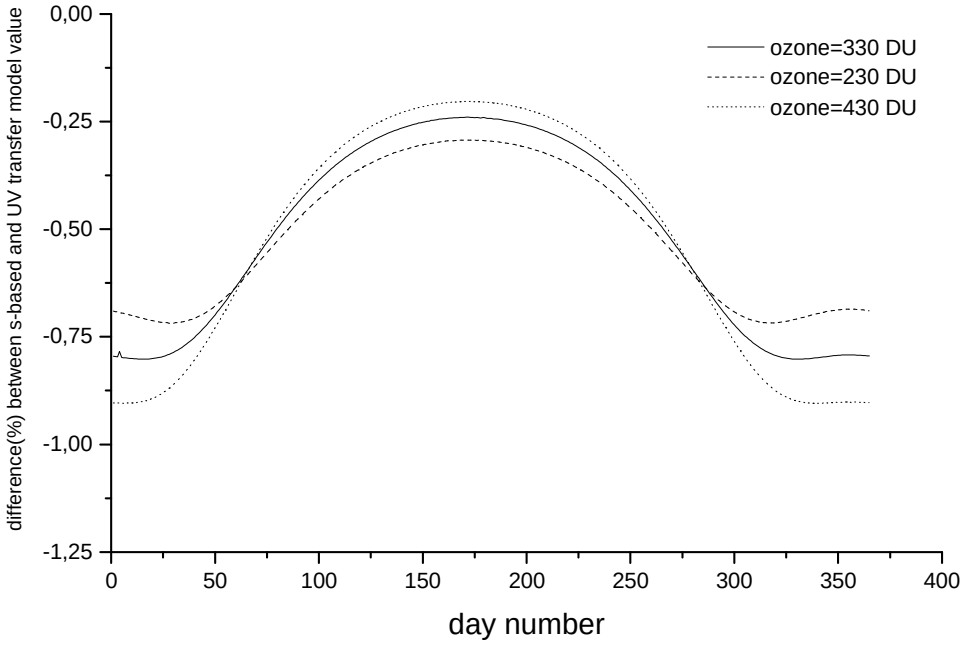

Figure 4.19 Difference in effective UV at τ=0.0 based on S calculated at 330 nm and calculations with the UV transfer model, for ozone concentration varying from 230-430 DU. Location: De Bilt.

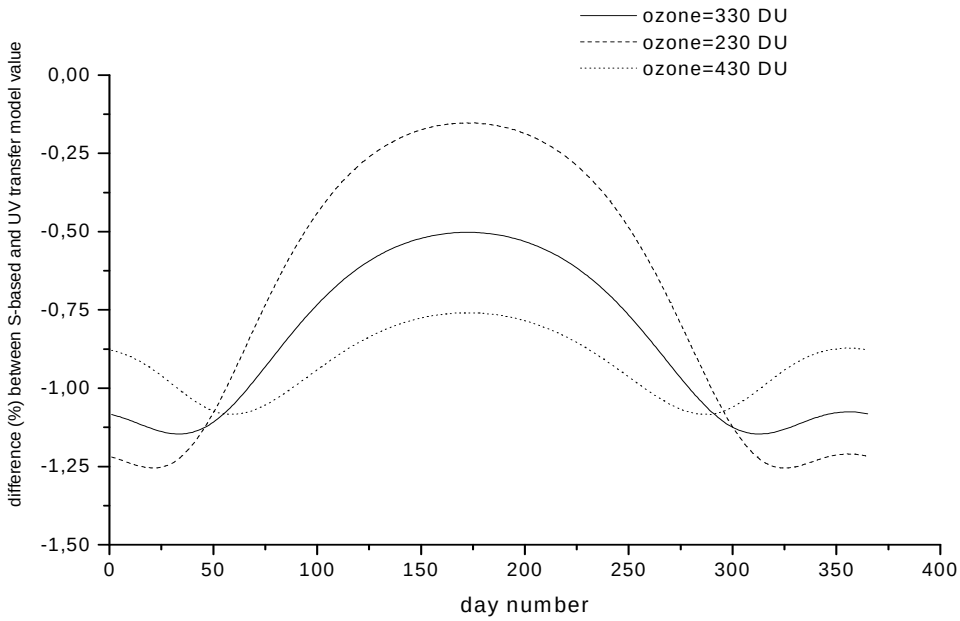

Figure 4.20 Difference in effective UV at τ =1.0 based on S calculated at 330 nm and calculations with the UV transfer model, for ozone concentration varying from 230-430 DU. Location: De Bilt.

From figures 4.19 and 4.20 we conclude that over the τ range (0.0-1.0) the differences between S-based effective UV and modeled value range from 0 to1.25%. For our purpose, a first approximation of the aerosol effects, an inaccuracy of just over 1% is quite acceptable.

4.3.4 Dependence of S on location

Finally, the S parameter depends on the location (longitude and latitude). We checked the dependency for three locations: De Bilt (5.2 W, 52.1 N), Arjeplog (Mid-Norway, 18W, 66N) and Madrid (4E, 40N). A first attempt to work with a location independent S introduced too high inaccuracies (-4% to +2%), relative to calculations with the UV transfer model. However, if we use a location dependent S we again get quite acceptable estimates for the S-based effective UV (inaccuracy ranging from –1.2% to -0.2%, see figures 4.21 and 4.22).

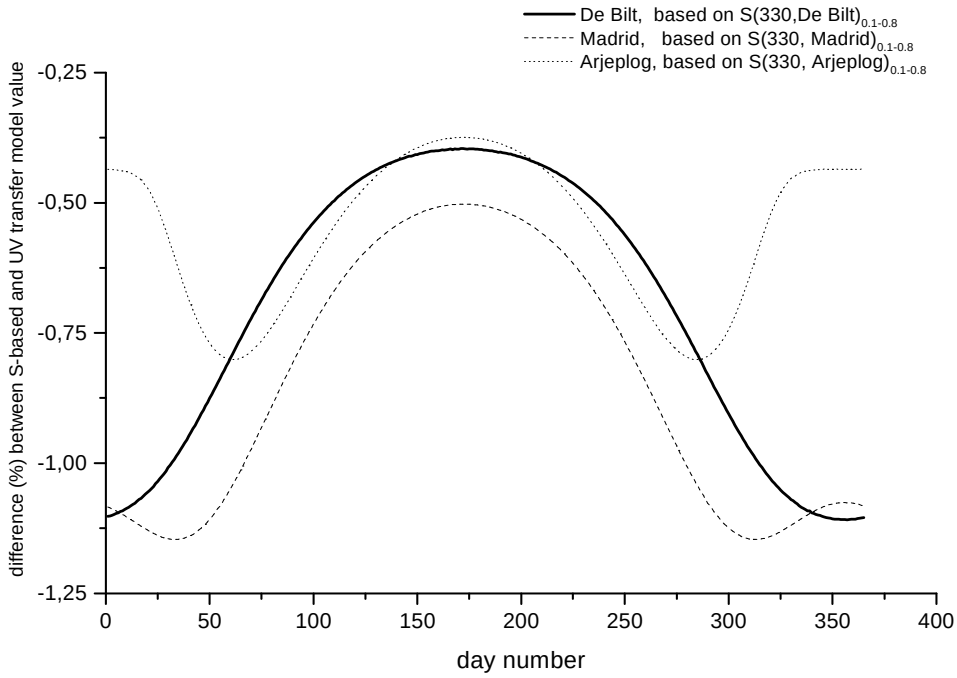

Figure 4.21 Difference in effective UV at τ =1.0 based on S calculated at different locations (and 330 DU) and calculations with the UV transfer model.

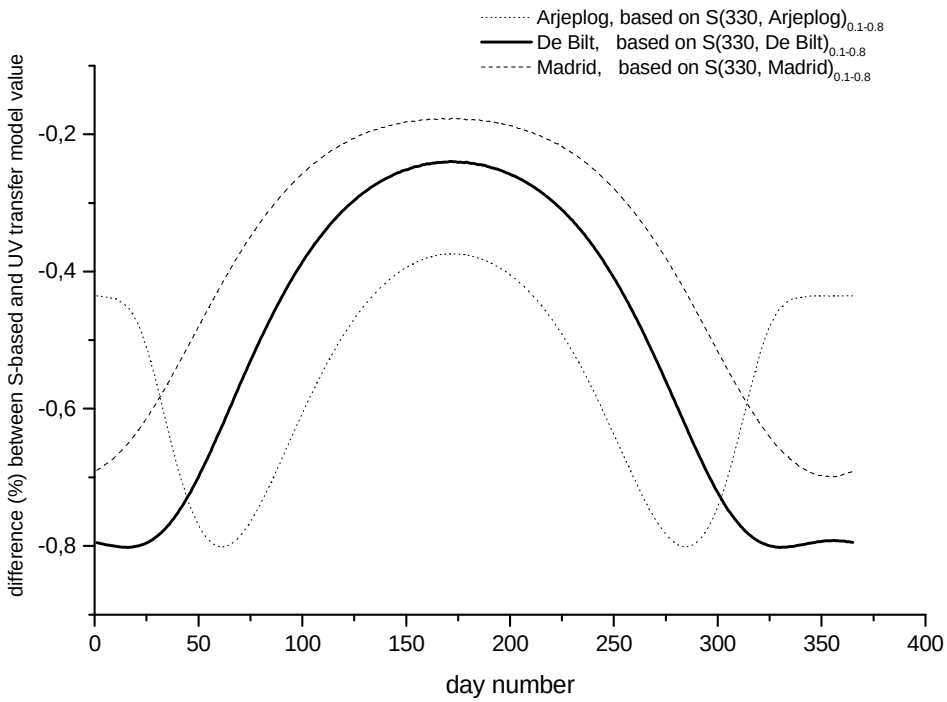

Figure 4.22 Difference in effective UV at τ =0.0 based on S calculated at different locations (and 330 DU) and calculations with the UV transfer model.

As a consequence we can employ a daysum and location dependent S to account for the effects of variable aerosol concentration. With a fixed aerosol optical thickness our UV budget mapping procedure is based on the computation of just one lookup table at the chosen aerosol optical thickness. Incorporating temporal and spatial variation in aerosol content adds up to computation of two lookup tables (one extra). One for τ =0.1 and a second for τ =0.8. These lookup tables enable us to compute a S-parameter for every location and for every day. The effective UV at τ =0.1 for the given location and day in combination with the actual local aerosol optical thickness (τ) finally yields – via equation 4.8 - the effective UV dose at the given location and day corrected for the different local aerosol optical thickness. This roughly implies doubling of our computation time.

4.3.5 Availability of time and space resolved aerosol data for Europe

In this section we developed a method to include temporal and spatial variations in aerosol optical thickness in our calculations of UV budget maps for Europe. Unfortunately, in contrast to the albedo we do not have a comprehensive data record with temporal and spatial resolved aerosol data. At present we do not even have a data record which could be regarded as a first approximation to such a high resolution data set. Moreover we do not have any experimental data on effective UV in dependence of aerosol concentration. Consequently, we cannot validate our method for aerosol variation against experimental data, nor can we evaluate the effect of variation in aerosol optical thickness over Europe on our UV budget maps.
Hopefully time and space resolved data on aerosol optical thickness for Europe will become available in the near future as a result of new remote sensing techniques in combination with a more sophisticated analysis of the satellite data records.

4.3.6 Conclusions on aerosol effects

The effect of variation in aerosol concentration can be implemented in our UV budget mapping on basis of the S-parameter introduced in equation 4.7. Inaccuracy in the estimate of effective UV based on the S is maximal 1-2% relative to the effective UV computed with the UV transfer model. Accounting for temporal and spatial variation in aerosol optical thickness requires computation of one extra lookup table in our present mapping procedure, roughly doubling total computation time.
Due to the lack of aerosol data with sufficient temporal and spatial resolution, we can at present not visualize the effect of variation in aerosol optical thickness in the UV budget maps for Europe. However, the developed method yields a rough estimate for the influence of aerosol optical thickness on effective UV. For every 0.1 increase in aerosol optical thickness, τ, the ground-level effective UV will decrease by approximately 3%.

4.4 Effects of variable tropospheric ozone load

4.4.1 Introduction

Ozone in the troposphere reduces the UV flux at the earth surface. Especially during summer smog periods the effects may be non-negligible. Consequently, it is important to account for temporal and spatial differences in ozone concentrations in the troposphere over Europe. In the context of the SULPHATE project, a method has been developed at IVM (Amsterdam) to include differences in tropospheric ozone in the UV-transfer model (see 2.6). This method calculates the sensitivity (S) of effective ultraviolet for the change in tropospheric ozone content. The S-parameter is mainly dependent on the solar zenith angle and on the total vertical ozone column thickness. Based on the look-up table for effective UV (see 2.1), the difference of the actual tropospheric ozone load an the ozone content of the standard troposphere, and the S-parameter, the effective UV can be calculated. Starting from the IVM-approach we face the same problem as with the aerosol correction. Basis for the UV mapping procedure forms the computation of effective UV daysums which requires adaptation from the IVM method. We here present and validate a method based on the sensitivity parameter S (defined in analogy to IVM) which yields adequate estimates of the influence of variation in tropospheric ozone on the daily effective UV dose.

The sensitivity parameter S' is determined by the effective UV daysums at two values of ozone in the troposphere, UV_0 at O_{30} and UV_1 at O_{31}. We base our approach on the total amount of ozone in the troposphere (defined as all heights below 12 km.). The S'-parameter is defined as:

$$S'(\text{day}) = \frac{\ln(UV_0) - \ln(UV_1)}{O_{31} - O_{30}} = \qquad (4.9)$$

This S'-parameter is used to estimate the effective UV daysum at tropospheric ozone = O_3 (DU)

$$UV_{est}(O_3) = UV_0 * \exp\left((O_{30} - O_3) * S'(\text{day}) \right) \qquad (4.10)$$

Eventually the check is made on the difference (in terms of percentage) between the estimated UV daysum on basis of the S' parameter and the daysum computed directly from the UV transfer model ($UV_{mod}(O_3)$).

$$\text{Difference (\%)} = 100 * \left(UV_{est}(O_3) - UV_{mod}(O_3) \right) / UV_{mod}(O_3) \qquad (4.11)$$

Starting point for the variation in tropospheric ozone is our standard ozone profile at a total ozone column of 330 DU. In our standard profile about 40 DU is contained in the troposphere. For the variation in tropospheric ozone concentration we chose a range from 20 DU- 60 DU. The rest of the ozone profile (above 12 km) is kept identical. Thus ozone variations in the troposphere are uncoupled from the ozone content and ozone profile in the stratosphere. On balance this implies that the total amount of ozone increase with the same amount as the ozone in the troposphere. Figure 4.23 depicts the five ozone profiles used in our calculations.

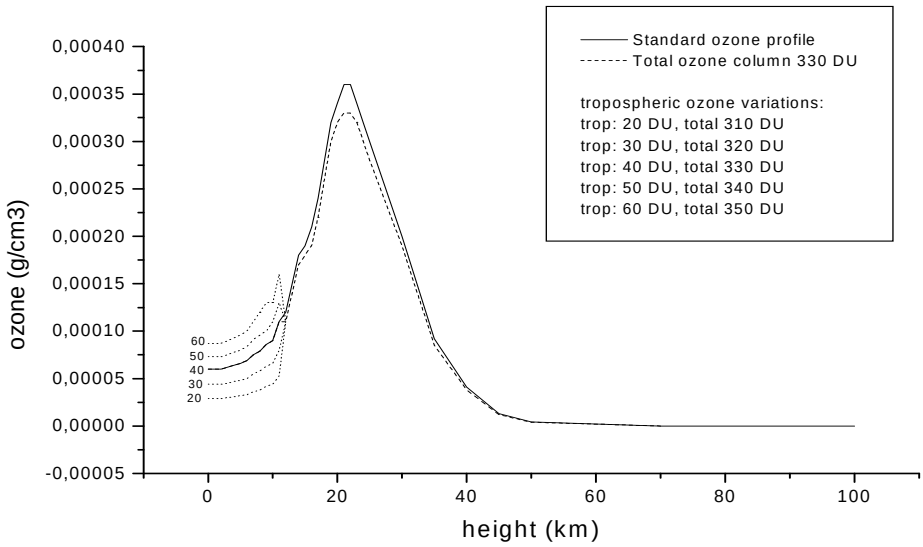

Figure 4.23 Ozone profiles used to assess effects of increase in tropospheric ozone. Tropospheric ozone varies between 20 DU and 60 DU. Stratospheric ozone content is fixed at 290 DU.

4.4.2 Dependence of S' on tropospheric ozone content

The S'-parameter is determined by the choice of the two string point for tropospheric ozone concentration O_{30} and O_{31}. We chose O_{30}= 30 DU and O_{31}=50 DU, and use the S' to estimate the effective UV daysums at 20 DU, 40 DU and 60 DU (tropospheric ozone content). The behaviour of S' in dependence of the day number is plotted in figure 4.24

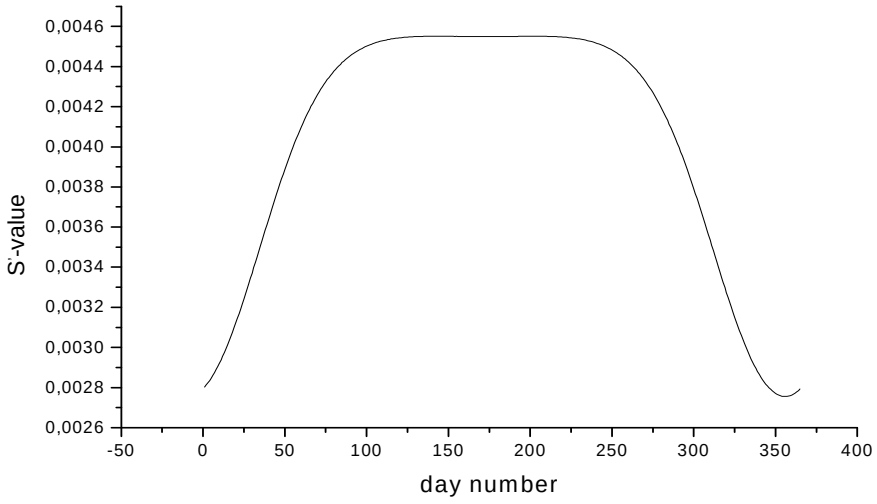

Figure 4.24 S'-parameter for influence of tropospheric ozone concentration on effective UV daysums, string points O_{30}= 30 DU and O_{31}=50 DU.

The year averaged S' is 0.004, pointing to a small influence of tropospheric ozone on the effective daily UV, of approximately 4% decrease in effective UV for every 10 DU increase in tropospheric ozone content.
Finally, we checked how accurate the S'-based method estimates the effective UV daysum. We compared the S'-based estimate for effective UV with tropospheric ozone = 20 DU, 40 DU and 60 DU to the estimate calculated with the UV transfer model values. (see figure 4.25)

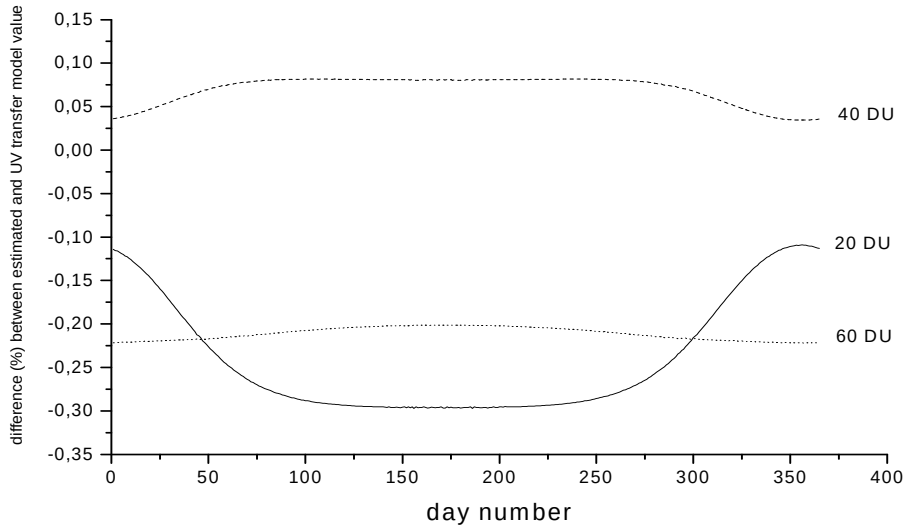

Figure 4.25 Comparison of effective UV daysums based on the S' and based on direct calculations with the UV transfer model for tropospheric ozone contents of 20, 40 and 60 DU.

On basis of figure 4.25 we conclude that the S'-parameter defined in equation 4.9 gives a sufficient accurate estimate for the influence of stratospheric ozone on the effective UV. The accuracy over the ozone range investigated is between –0.3% and +0.1% difference relative to the effective UV calculated with the UV transfer model. To implement the variation in tropospheric ozone we have to compute two lookup tables (one extra as compared to the standard UV budget mapping procedure) for a tropospheric ozone content of 30 and 50 DU. These lookup tables enable us to compute the parameter for tropospheric ozone change at a given day, and location. This S' combined with the daily effective UV and the actual local tropospheric ozone concentration yields the corrected UV dose according to equation 4.10. The cost of incorporating the effects of tropospheric ozone is roughly a doubling in computation time.

4.4.3 Availability of temporal and spatial resolved data on tropospheric ozone for Europe

The missing link to account for variation in tropospheric ozone is a record with time and location dependent data. Unfortunately such a data set is missing at the moment. There are some data on tropospheric ozone for summer smog periods. But in these cases measurements are restricted to ground-level and do not give information on the whole troposphere. And

these data are only available at a few, irregular time point over the year, for some locations in Europe. LIDAR measurement are more or less routinely performed and may turn out to be a valuable source of data on tropospheric ozone. At present, tropospheric ozone is not routinely reported. A more serious drawback is the small amount of LIDAR measuring stations in Europe. Apart from the lack of ozone data we do not have any (local) measurements of effective UV for different tropospheric ozone contents. As a result, we cannot validate our method for tropospheric ozone variation against experimental data, as we could in the case of variations in surface albedo. In the absence of a comprehensive data record with sufficient temporal and spatial resolution for Europe we can not calculate the effect of variation in tropospheric ozone concentration over Europe on our UV budget maps.
Hopefully, in the near future remote sensing techniques like LIDAR or tailor-made satellite instruments will produce high resolution data – with respect to time and space – on the distribution and content of ozone in the troposphere. These measurements may, in combination with improved data analysis, result in an adequate comprehensive record on variations in tropospheric ozone over Europe.

4.4.4 Conclusions on the effects of tropospheric ozone

The method on basis of the S'-parameter (introduced in equation 4.9) is adequate to incorporate temporal and spatial variations in tropospheric ozone content in our UV budget mapping procedure. Inaccuracy in the estimate of effective UV based on the S' is less than 0.3% , relative to the effective UV computed with the UV transfer model. Accounting for temporal and spatial variation in tropospheric ozone asks for the computation of one extra lookup table in our present mapping procedure, roughly doubling total computation time.
Due to the lack of data on tropospheric ozone content with sufficient temporal and spatial resolution, we can at present not visualize the effect of variation in tropospheric ozone concentration in the UV budget maps for Europe. But the method used gives us an indication of the magnitude of the effects. For every 10 DU increase in tropospheric ozone content a decrease in effective UV of approximately 4% is to be expected.

5 UV-climatology and trends in Europe in relation to ozone changes

5.1 Introduction

Public concern about stratospheric ozone depletion led in 1985 to a first framework for international restrictions on the production and use of halocarbons, the so-called Vienna Convention. The first estimate of the reduction in skin cancer rise resulting from these restrictive measurements was given by Slaper et al. [Slaper et al., 1996]. However, these estimates were based on an ozone trend averaged over the Northern Hemisphere (mid-latitudes) of –3.9% per decade [WMO, 1995]. From our UV mapping method we can extract geographically resolved ozone trends based on TOMS ozone data. In this paragraph we present the first result on these ozone trends. In future research these ozone trends will be used for skin cancer prognoses, in relation to restrictive scenarios for production of halocarbons, at different locations in Europe.

5.2 Methods

To assess the effect of restrictive scenarios on the induction of skin cancer we must use a model that integrates the full source-risk chain: from the production and emission of halocarbons through ozone depletion and increase in UV radiation up to the increase in skin cancer incidence. The model includes dynamical aspects of skin cancer induction, e.g. a latent period between exposure and tumour development. The three types of skin cancer, associated with UV exposure, are included: squamous cell carcinoma (SCC), basal cell carcinoma (BCC) and cutaneous malignant melanoma (CMM). BCC is the most common, but least aggressive form of skin cancer. SCC is less common but has a higher tendency to metastasize. CMM is the least frequent skin cancer, but the most aggressive form (see also § 2.5, table 2.2). For the baseline incidence in northwest Europe we use data for the Netherlands. These data given in table 2.2 indicate a total incidence of about 1200 new cases of skin cancer per one million inhabitants per year.
We compare two restrictive scenarios under the Vienna Convention (Montreal protocol and Copenhagen amendments) with a ‘no-restrictions’ scenario. In the no restrictions (NR) scenario we assume an ongoing 3% annual increase in the production of ozone depleting substances (chlorofluorocarbons, halons and methyl chloroform). In the Montreal protocol scenario (MP, 1987) the production of the five most potent ozone depleting substances is reduced to 50% by the end of 1999. In the much stricter Copenhagen amendments (CA, 1992) the decline in of production of ozone depleting substances is much faster. A reduction of the production of the 21 most potent ozone depleting substances to virtually zero at the end of 1995 is aimed at. We assume full global compliance to the scenarios given. Furthermore we assume that the sun exposing behaviour of the population is the same for all scenario’s.
The emitted halocarbons at ground-level are transported to the stratosphere where the photochemical breakdown releases active chlorine and bromine. These free radicals act as a very effective catalyst for ozone destruction. The observation that the downward trends in ozone started a few years after the elevation of chlorine levels suggest that ozone destruction only began after a certain threshold in chlorine had been reached [Daniel et al.,1995 , WMO, 1992]. Above this threshold observations and modeling of the stratosphere suggest a linear relationship between chlorine loading and relative decrease in ozone column [Velders, 1995].

At very high chlorine levels ozone in the lower parts of the stratosphere is virtually fully destroyed, and saturation of the ozone depletion is expected [Kerr, 1995]. As reference period to determine ozone trends over Europe we take the 12 year period 1979-1991. For this period an uninterrupted ozone record of NIMBUS7 aboard the NASA TOMS is available. We do not include 1992 in our analysis because of the impact of the Pinatubo volcano on atmospheric properties. Skin cancer induction is described by the method introduced in § 2.5

5.3 Results

Figure 5.1 depicts the ozone trends – based on year averaged ozone, for 1979-1991.

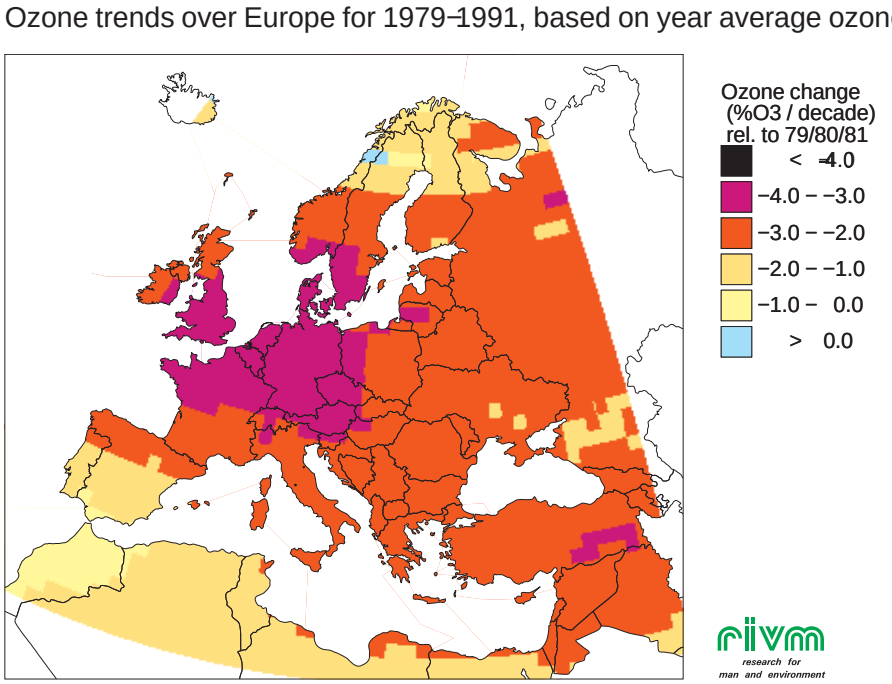

Figure 5.1 Ozone trends for the period 1979 - 1991 over Europe. Trends are expressed as a percentage change per decade, relative to the average ozone column thickness for the years 1979, 1980 and 1981.

The trend map shows a consistent decrease in ozone column thickness, typically ranging from –4% to -1% depletion of the ozone column per decade. The only exception being a small region in north-west Norway, with a small statistically insignificant positive ozone trend. The highest decrease in stratospheric ozone is found over central north-west Europe, including the Netherlands. The ozone decrease over this region is (roughly) consistent with the trend reported by the WMO of –3.9% per decade [WMO 1995]. Ozone trends vary substantially over the months of the year. Moreover, the distribution of the ozone trend over the months is needed as input for the UV chain risk model. Therefor ozone trends for all the months of the year were calculated. Figure 5.2 and 5.3 give monthly ozone trends for April and August.

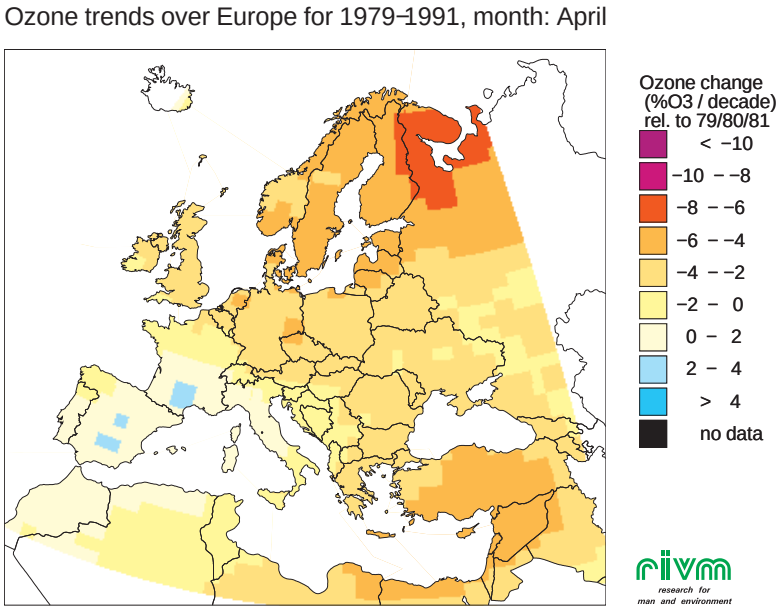

Figure 5.2 **Ozone trend over Europe, during spring. Ozone trend is expressed as a percentage per decade, relative to the average ozone column thickness over 1979, 1980 and 1981**

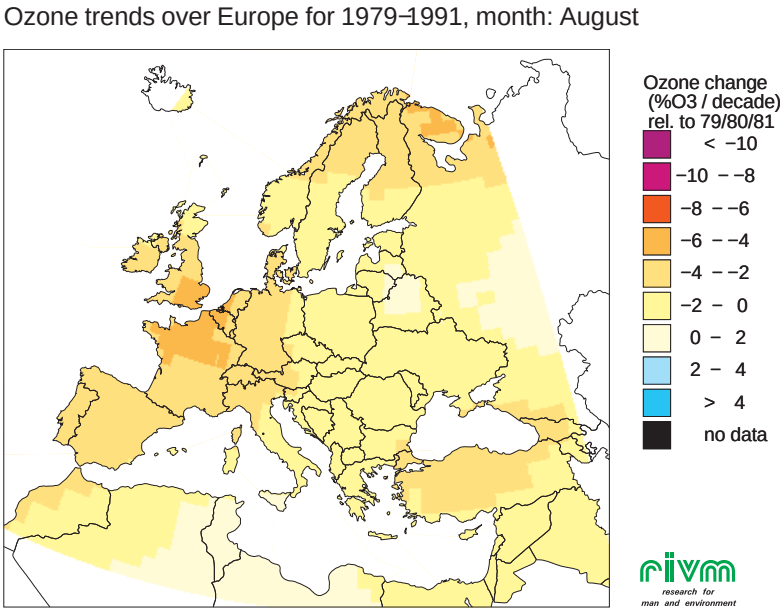

Figure 5.3 **Ozone trend over Europe, during summer. Ozone trend is expressed as a percentage per decade, relative to the average ozone column thickness over 1979, 1980 and 1981.Figure 5.3**

Monthly ozone trends are much more variable than the year average. Positive ozone trends occur all over Europe in a somewhat unpredictable way. This monthly ozone trend maps yield essential information for the UV chain risk model. This model requires the following input data: ozone trends over the given period for every month of the year, the ozone value at the start and the ozone value at the end of the considered period. As starting point we use the average ozone concentration over the years 1979, 1980 and 1981. As endpoint we use the average ozone value for the year 1991. Finally we need the baseline UV. For this dose we chose the clear-sky UV averaged over 1979, 1980, 1981.

Ozone trend for four typical location in Europe (selected on basis of figure 5.1) are given in figure 5.4. We chose four locations with different yearly ozone trends to evaluate which differences in risk prognosis were associated with the observed ozone trend differences. One location in Morocco (5 E, 35 N), one in Mid-Spain (5 E, 39 N), one in South France (0, 44N) and the last in The Netherlands at De Bilt (5.2 W, 52.1 N).
Figure 5.4 gives the local ozone development, on basis of year average ozone, over the period 1979-1991 for the four locations given, and the best fitted trend lines.

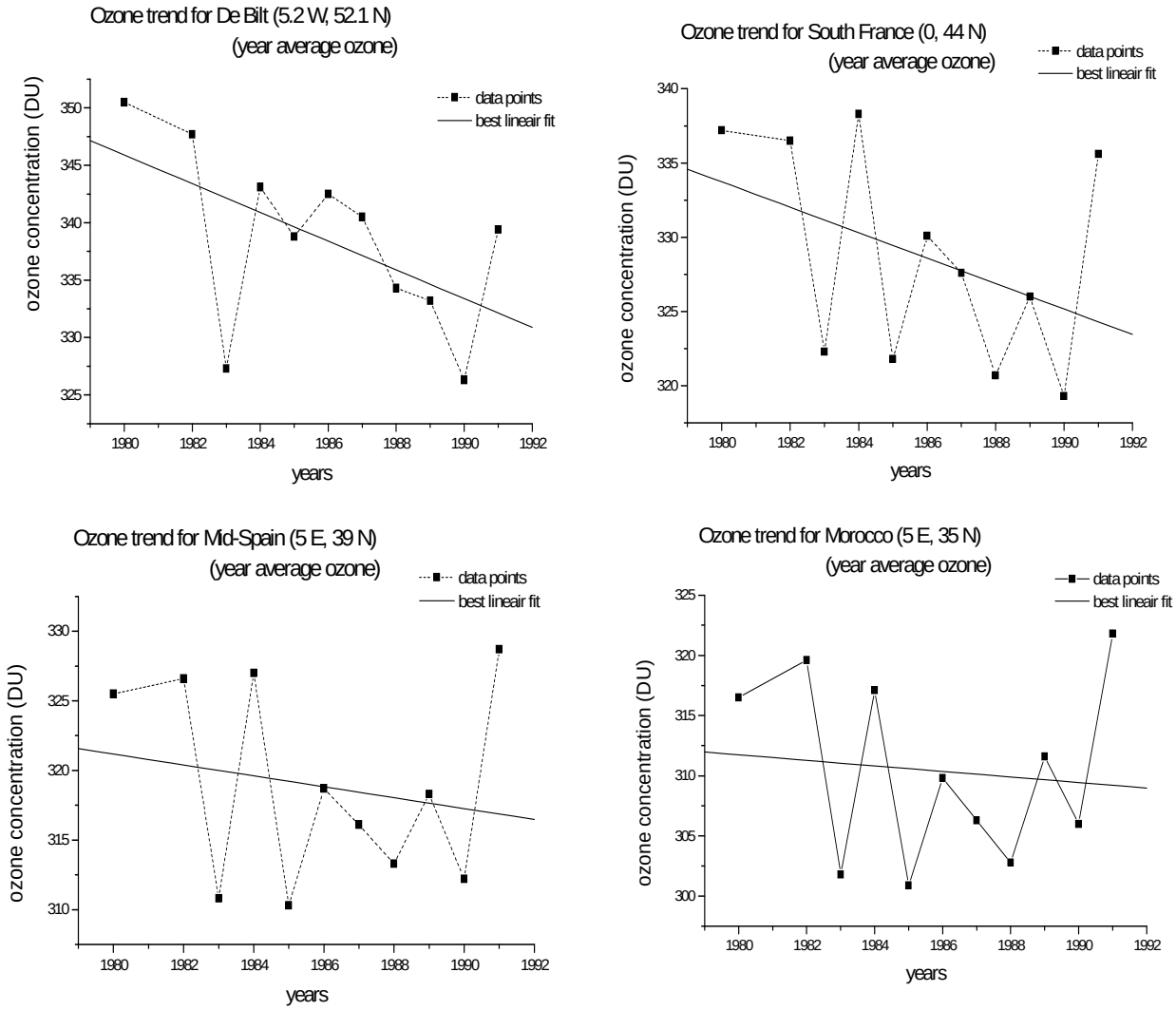

Figure 5.4 Ozone trend – based on year average ozone for four different locations in Europe

Ozone concentrations show substantial year to year variations. As a result ozone trend analysis does not yield a significant negative trend for all locations (see table 5.1). In table 5.1 we give additional data on monthly ozone trends, yearly average ozone concentration and effective UV. Monthly ozone trends show a much higher variability. Before we can use these ozone trends as input for calculations with our UV-chain-risk model further analysis is required.

Table 5.1 Ozone and UV data needed as input for the UV chain-risk-model

Location	Netherlands	South-France	Mid-Spain	Morocco
Ozone trend	% / decade	% /decade	% / decade	% / decade
Year average	-3.6 ± 1.7	-2.5 ± 1.9	-1.2 ± 2.0	-0.7 ± 2.2
January	-5.5 ± 7.7	-1.6 ± 5.3	-0.8 ± 5.0	-1.1 ± 4.5
February	-0.9 ± 5.5	-4.8 ± 6.4	-3.5 ±5 .7	-2.5 ± 6.2
March	-8.4 ± 5.1	-8.9 ± 4.6	-4.0 ± 6.0	-4.0 ± 5.5
April	-4.0 ± 3.3	+1.2 ± 4.2	+1.8 ± 4.0	+1.1 ± 4.1
May	-5.4 ± 3.5	-5.0 ± 4.2	-2.6 ± 4.2	-0.7 ± 4.3
June	+1.6 ± 3.2	-0.6 ± 2.7	+0.8 ± 3.4	+1.6 ± 2.4
July	-1.9 ± 2.3	-1.4 ± 2.0	-1.0 ± 2.0	+0.8 ± 2.3
August	-3.6 ± 2.0	-3.3 ± 1.5	-2.8 ± 1.7	-2.5 ± 2.0
September	-1.7 ± 1.7	+1.4 ± 2.4	+0.5 ± 2.1	-0.9 ± 1.8
October	-5.2 ± 2.9	-2.3 ± 1.5	-0.6 ± 2.5	-0.9 ± 2.2
November	+0.9 ± 4.4	+1.3 ± 3.0	+1.0 ± 2.2	+3.6 ± 1.8
December	-7.5 ± 4.1	-5.3 ± 3.3	-3.1 ± 3.0	-2.9 ± 2.3
Ozone1979/1980/ 1981 (DU)	350.5	337.2	325.5	316.5
Ozone 1991 (DU)	339.4	335.6	328.7	321.8
Effective UV 1979/1989/1981 (SCUPh, MJ/m²)	1.45	1.97	2.44	2.79

In analogy to the ozone trends we computed the ultraviolet trends and the average UV over Europe. The trends are based on yearly effective UV doses computed with our UV transfer model on basis of the TOMS data (see chapter 2). In the period 1979-2000 we have 18 years of TOMS data at our disposal. For the period 1993-1996 no full data set is available. Figure 5.5 illustrates the average effective UV. Figure 5.6 the UV change per decade.

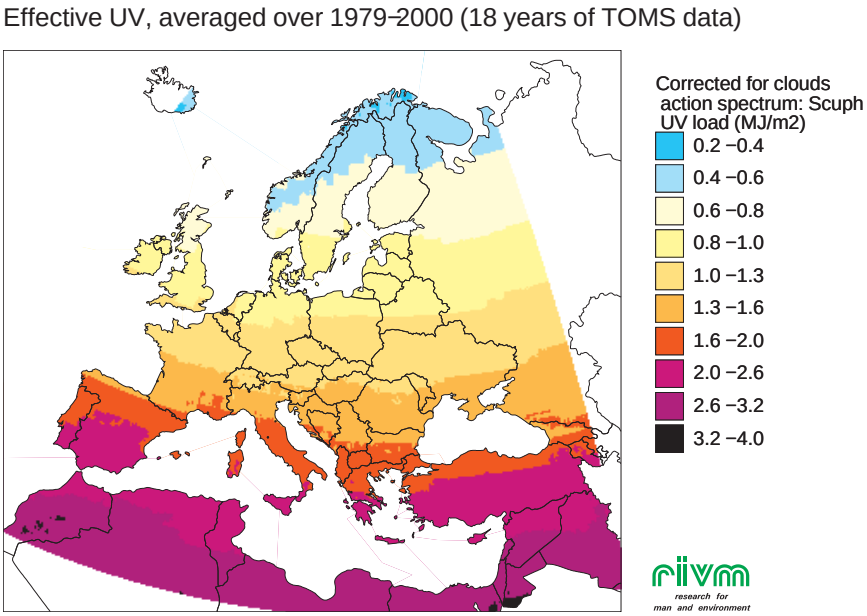

Figure 5.5 **Average effective ultraviolet over Europe corrected for clouds, for the period 1979-2000. Years for which no full TOMS data are available (1993-1996) have not been taken into account.**

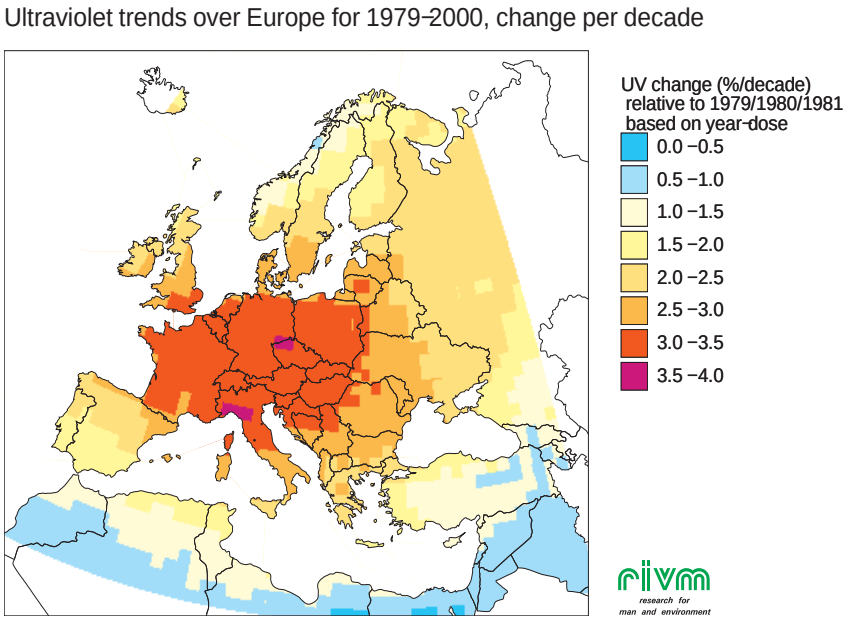

Figure 5.6 **Ultraviolet trend over Europe based on yearly effective UV under clear sky conditions. The UV trend is expressed as a percentage change per decade, relative to the average effective UV over 1979, 1980 and 1981.**

5.4 Discussion and future development

Year average ozone trends calculated in this chapter point to a consistent ozone depletion over Europe, with ozone trends ranging from –1% to - 4% O_3 per decade. Monthly ozone trends are highly variable and not negative for all months at all locations. Before we can use these monthly ozone trend data in the UV-chain-risk model a thorough evaluation of the uncertainties has to be performed. Thereafter we will use the geographically resolved ozone trends – at least if they are sufficient reliable - to calculate prognosis for the skin cancer risk in 2100 under the different ozone depleting scenarios in the framework of the Vienna convention. Ultraviolet trends over Europe range from 0.5 to 4% per decade. The highest upward trends are calculated in the central part of Western Europe.
It should be noted that ground based analysis including the years 1993-1996 (the period without data in the TOMS record) results in larger UV-trends as compared to ground analysis omitting this years. Therefor, the satellite based calculations may underestimate the UV trends.

6 Cost/benefit of the remote sensing approach

6.1 Introduction

To asses the present and future risks associated with human UV exposure we need detailed information on the location dependent, ground-level UV, the (spectral) composition and change in UV-irradiance over the past decades and information on possible future changes in the UV at ground-level. From the perspective of development (and evaluation) of environmental policy we need to know to what extend this UV change is the result of human action, as only man-made changes can be counteracted by specific policies. In practical terms this means we must be able to separate the man induced ozone change from 'natural' changes due to year-to-year variation, clouds, volcano's, etc.
UV irradiance at the earth's surface can be assessed by:

- '*ground-based measuring'*
  determining the effective UV by direct, spectrally resolved measurement of UV-irradiance at the ground;
- *'ground-based modelling'*
  determining effective UV by transfer model calculations supplemented with ground-based ozone column measurements and ground-based cloud observation;
- *'satellite-based modelling'*
  determining effective UV by transfer model calculations in combination with satellite-based observation of ozone column and cloud reduction;

These three methods employ remote sensing to different extends. The first is totally based on local measurements on the ground. The second is based on model calculations, in combination with ground-based measurements, although ground-based measurements of stratospheric ozone is in fact a remote sensing technique too. The last method can be fully performed with remote sensing techniques and model calculations.
In this section we compare the merits of the remote sensing approach with the ground-based methods.

6.2 Remote sensing techniques versus ground-based measurements

To compare the satellite-based modelling with the ground-based measuring and ground-based modelling we evaluate the following aspects: time coverage, temporal resolution, spatial coverage, spatial resolution, ozone influence, accuracy, stability and data availability.

6.2.1 Time coverage

Risk estimates for humans usually focus on skin cancer. As the development of skin cancer may take several decades up to a lifetime we have to look back on the exposure history of the population. In other words, we need estimates for UV budgets at least twenty years back The TOMS record extends from 1979 till now, with a gap for the period 1993-1996. Other satellites supplement the TOMS record for ozone or cloud cover data, for instance the GOME satellite (data available since 1986). Meteo satellites may add data on cloud cover, for instance the ensemble of satellites combined in the ISCCP project. Ground-based ozone

measurements are available more than 20 years back, for a limited number of ground-stations. The KMI station in Ukkel (Belgium) for instance has a data record starting in 1971. The ozone measuring method is accurate and stable, yielding reliable data for a trend analysis. Cloud cover data can be calculated from global radiation measurements which has been performed routinely over a prolonged time period and for a extensive network of ground-stations. So time coverage of satellite-based and ground-based modelling is comparable. In the case of 'ground-based measuring' time coverage is worse. UV measurements with sufficient stable and accurate instrumentation are only available starting 5 – (maximum) 10 years back. Although initiatives from the European Union for intercomparison of measuring techniques and a European database for (spectral) UV-measurements will improve the situation in the coming years, the historical gap can not be filled. The 'ground-based measuring' will therefor cover a smaller number of years as compared to the modelling methods. In addition to spectral UV measurement erythemally weighted UV has been measured routinely, for over 25 years at a high number of locations with Robertson-Berger (RB) meters [Borkowski, 2000, Weatherhead et al., 1997]. However, the stability of the RB-meters does not allow for a reliable UV trend analysis [Borkowski, J.L, 1997].

6.2.2 Temporal resolution

Ground-based measuring yields the highest temporal resolution. Usually several spectra are measured every hour, resulting in a temporal resolution in the order of minutes. Ground-based ozone measurements are normally performed one or a few times per day, yielding a temporal resolution in the order of hours. The TOMS satellite has one daily overpass only, giving a temporal resolution of one day for the ozone and reflection measurements. Other satellite may have different characteristics. ISCCP for instance produces cloud cover data every three hours (but no ozone data).

6.2.3 Spatial coverage

On the aspect of spatial coverage the advantage of satellite-based methods is evident. Satellites measuring ozone and reflection data usually give global coverage, whereas ground-based measuring and ground-based modelling is restricted to only a few ground-stations with adequate instrumentation.

6.2.4 Spatial resolution

In theory, 'ground-based measuring' techniques and ground-based modelling can yield an ideal spatial resolution, because the data are uniquely linked to the measuring location. In practical terms, resolution is usually poor due to the low numbers of ground-stations measuring ozone and/or UV data. But, in situations where the spatial variation of the UV is not very high, one ground-stations is representative for the whole region surrounding it. Spatial resolution of the ground-based approach can be easily improved by increasing the number of ground-stations. For satellite measurements the spatial resolution is low, even theoretically, because the satellite high above the earth's surface inevitably averages the information over some surface area (1.25° x 1.0° (latitude x longitude) cells for the TOMS). Improvement of spatial resolution requires sophisticated adjustments to the instrumentation. In theory, spatial resolution of the ground-based methods is better. In practical terms the resolution of the satellites is not inferior to the ground-based methods. Consequently we judge al three methods as more or less (+/-) adequate to the aspect of spatial resolution.

6.2.5 Ozone influence

From the viewpoint of environmental policy, it is crucial to separate man-made influences (mainly ozone depletion) on UV budgets from natural causes. Ground-based UV measurements produce an UV budget with the effect of environmental influences (ozone, aerosols, albedo, clouds) pooled together. Some effects can be calculated on basis of the measured spectra. The ratio UVB/UVA, for instance, can be used to estimate the ozone influence. Other properties, like cloud cover can be assessed on basis of additional data. Both satellite-based and ground-based modelling use a direct, separate measurement for ozone column thickness. Therefor both methods can readily account for ozone influences separately.

6.2.6 Accuracy

Spectral measurements of the UV irradiance at the ground still yield the most accurate determination of the actual, local UV-dose (inaccuracy 3-5%). For both other methods the type of transfer model used will introduces an inaccuracy and the way in which ozone concentration is determined (from satellite-data or from ground-based measurements) will introduce an extra inaccuracy. Effective UV year doses computed from satellite-data (TOMS overpass) and ground-based ozone measurements do not show substantial differences in accuracy [Slaper et al., 2001].

6.2.7 Stability

Since the mid-nineties spectral UV measuring instruments with sufficient stability have become available. However calibration of the instrumentation remains a time consuming and complicated process, prone to instrumental and human error. For the satellite-based and ground-based modelling good stability has been shown, mainly because the used techniques are relative, over a prolonged period (1979-1998, [Slaper et al., 2001).

6.2.8 Availability

A last point of interest is how easily and how fast data become available. Availability of TOMS data is almost real-time and all data can easily be downloaded from the NASA ftp-site. For other satellite sources this may be different. For ISCCP, for instance, it takes several years before validated data become available. Ground-based ozone measurements are usually readily available from the ground-stations. In our case the Ukkel data are available at the ftp-site of KMI within two weeks.
At present, direct UV measurements are not so easily obtained. All institutes employ their own instrumentation and measurement protocols, making data exchange – apart from during intercomparison campaigns - complicated. Recently, in the context of the SUVDAMA project a first attempt to install a European database was undertaken. In the near future, the EU initiative to set up a European data base for UV measurements may result in a much better availability and comparability of (European) UV measurements.

6.2.9 Cost estimate

Introduction
The total costs to produce UV–budget maps, based on remote sensing data or on ground measurements, consist of the costs for producing the basic data and of the costs for the end-user to access the data, to process the data into budget maps and to store data and results (data management). The production costs for the basic data can be divided into ‘hardware costs’

(development, production and installing of the instruments) and into operational costs (operating and calibrating the instruments and quality control of the data). In the case of remote sensing, hardware costs encompasses development and production of the sensor, the platform, the satellite and launching of the satellite. For a future (European) ground based UV measuring network, hardware costs arise mainly from developing, purchasing and installing instrumentation (radiometers, monochromators, pyranometers, computers). Just to be perfectly clear, a European network of UV measuring sites with adequate coverage is at present not available and will probably not be available in the near future, although in the framework of the EDUCE-project - in which RIVM participates - the first steps towards a European UV database are taken.
It is evident that the production costs of the basic data may be substantial, especially for the hardware. In this report we restrict ourselves to operational costs and to the cost of data management for the end-user.

Operational costs
For remote sensing operational costs are mainly for operating the ground segment and for provision of good quality data to the end-user. NASA's operational expenses for the ground segment of the TOMS mission amount to approximately 6.3 million EURO per year (5.7 million US$, averaged over 1997-1999, [NSTC, 1999]).
For a ground based network operational cost are the expenses for operating and calibrating the instruments, for control of data quality, for assembling the data into a database and for intercomparisons of different ground stations. For one measuring site we estimate a yearly cost of about 100.000 EURO. For a European network with a reasonable coverage at least 100 measuring sites are needed. Therefor, operational costs for such a network amount to roughly 10 million EURO per year.

Costs for data management
Usually end-users are only confronted with the costs for data management, because data are available for free from the internet. For remote sensing the data have a simple structure (for TOMS one ozone and one reflection measurement per grid cell per day) and data management is relatively simple. In this case costs for data exchange, model development and validation and data storage amount to 50.000 EURO per year (based on experience with UV budget mapping at the RIVM site).
For a ground based measuring network data structure is more complicated (50-100 spectra are produced per day for every location). Therefor, data handling and model development by the end-user will be more complicated and time-consuming. We estimate the total costs for calculating reliable UV-budget maps on basis of a ground based network at approximately 200.000 EURO for the end-user.

6.3 Conclusions on the remote sensing approach

In table 6.1 we summarise the findings of the previous paragraph..

Table 6.1 Overview of the merits of the three methods for assessing UV-doses

Aspect Method	Time coverage	Temporal resolution	Spatial coverage	Spatial resolution	Ozone influence	Accuracy	Stability	Availability
Ground-based measuring	-	+	-	+/-	+/-	++	+/-	+/-
Ground-based modelling	+	+/-	-	+/-	+	+	+	+
Satellite-based modelling	+	-	+	+/-	+	+	+	++

From the table it is obvious that none of the methods investigated is superior on all points. Therefor preference for one of the methods depends on the specific application. Our first goal is to generate adequate UV budget maps for Europe from the viewpoint of risk assessment and environmental policy. For this purpose the following properties of table 6.1 are of utmost importance: sufficient time and spatial coverage, good separation of ozone effects and good stability and availability. Table 6.1 shows that the ground-based modelling drops out (for mapping) because of the poor spatial coverage, and the ground-based UV measuring approach drops out mainly due to poor time and spatial coverage. For the UV budget maps we may therefor conclude that the satellite (TOMS) based remote sensing approach in combination with a UV transfer model is the most appropriate.

6.4 Application of UV-maps

The UV- and UV-risk maps have been included in a number of key publications on integrated environmental assessments from the European Environmental Agency (EEA) and the National Institute of Public Health and the Environment (RIVM). These key publications directly relate to the core tasks of the EEA and RIVM. The core responsibilities of RIVM are specified in the RIVM Act of 21 October 1996 and include:

- To carry out supportive research for governmental policy development and supervision of public health, nature, and the environment.
- To report periodically about the state of, and outlook for public health, nature, and the environment.

A statutory regulation in the Environmental Protection Act makes RIVM the environmental planning agency for the Dutch ministry of Housing, Physical Planning and the Environment (VROM). In this capacity RIVM compiles an annual Environmental Balance (Sheet), which describes to what extent changes in environmental quality development correlate to the environmental policy pursued, and an Environmental Outlook issued every four years, describing the environmental quality outlook in relation to policy goals for a period of at least the next ten years. The Environmental Outlook serves as scientific basic document for the

National Environmental Program.
In these integrated assessment reports UV budget maps show the increases in yearly UV-doses over the European continent related to decreases in ozone and/or the possible increases in skin cancer incidence associated with these changes. The results support the conclusions that it is very important to fully and globally comply with the countermeasures as described in UNEP's strictest Amendments of the Montreal protocol on Substances that Deplete the Ozone Layer, which were agreed upon in the context of the Vienna Convention to protect the ozone layer. For an overview of the environmental assessments in which the UV- and UV-risk maps have been used, we refer to pages 43, 44 of the CUBEO report [Slaper et al., 2001]. In addition to these national tasks RIVM serves as a Thematic Centre Air Quality, as part of the European Environmental Agency (EEA). The aim of the European Environment Agency is to establish a seamless environmental information system. This is done to assist the Community in its attempts to improve the environment and move towards sustainability, including the EU's efforts to integrate environmental aspects into economic policies.

Apart from these integrated assessments, UV budget maps have been used in the context of the Dutch National Research Programme on Global Air Pollution and Climate Change (NOP). In the NOP-project: ' impact of UVB irradiation on resistance to infectious diseases and efficacy of vaccination', UV maps have been used to visualize immune suppression caused by increased UV levels. UV budget maps are used in another NOP-project: 'Ozone and climate interaction effects for ultraviolet radiation and risks'. This project evaluates the effect of global warming on ozone recovery and UV levels over Europe.

Finally, the UV budget maps will play a role in the construction of a European database filled with (groundbased) UV data as is foreseen in the EC-fifth framework multilateral project EDUCE in which RIVM participates.

7 General Conclusions and Future Research

7.1 General Conclusions

Environmental changes affect the global UV climate. UV budget maps are useful to visualise ongoing changes in the UV climate over Europe. In combination with knowledge on the health effects of the UV radiation, the UV budget maps form a solid basis for risk assessments. UV budgets are not static with respect to time and place because effective UV at ground-level is influenced by a variety of (atmospheric) parameters. The major factors are: solar zenith angle, total ozone column and the distribution of ozone over the stratosphere and the troposphere, clouds, surface albedo, aerosol concentration and optical properties of the aerosols. These factors depend on season, time of the day, weather conditions and location. Insight in the relative effect of these parameters on the UV budget and information on their temporal and spatial properties is growing. However, at present a full determination of all these parameters with good temporal and spatial resolution is not achievable. This report is a step forward in the dynamical description of UV budgets, with time and place dependent (atmospheric) parameters. Additionally, it presents a first step towards a geographically resolved prognosis for excess skin cancer under the various scenario's of the Vienna convention for ozone depleting substances.

Main topics of this report are: cloud parameterisation, albedo effects, aerosols, tropospheric ozone and prognosis for excess skin cancer risk under the Vienna Convention. Finally, we performed a cost/benefit analysis of remote sensing methods.

Cloud parameterisation
Cloud cover and cloud optical properties are decisive for the actual UV budget at ground-level. We compared two cloud parameterisations based on satellite-data with ground-based reduction of global radiation. The first on basis of the ISCCP project, especially designed to develop a global cloud climatology with high temporal and spatial resolution. The second is based on the TOMS satellite, primarily tailored to produce ozone data. For both satellite-based methods the cloud reductions are in close agreement with the ground-based reduction. As a consequence ISCCP and TOMS both yield reliable data to calculate UV budgets under cloudy circumstances. For practical reasons, mainly data availability and time span covered, we employ the TOMS derived methodology in our mapping procedure.

Albedo effects
Properties of the earth's surface, especially snow cover, strongly influence the local UV dose. We developed a method to account for spatial and temporal variations in surface albedo. Albedo was extracted from monthly, long-term data for minimal reflectivity. In the winter in north-west Europe the albedo correction, for clear sky, results locally in a substantial increase in effective UV (30-40%). During summer the albedo correction is small, typically 0-2% for most parts of Europe. Accounting for variations in albedo does not substantially increase the clear sky yearly UV budgets, with the exception of north-nest Scandinavia and over high, snow covered mountains (increase in yearly UV budget of 6-8%).

Aerosols
Aerosol content and aerosol characteristics affect the local UV budget. Reductions in effective UV of 25% are possible, compared to an aerosol free atmosphere. We developed a

refinement of our UV mapping procedure to incorporate temporal and spatial differences in aerosol content. The increase in computational time for this refinement is acceptable and the calculated effective UV budgets do not deviate more than 2% from direct model calculations. Unfortunately, due to the lack of aerosol data for Europe with sufficient spatial and temporal resolution, the effect on the UV budget maps could not be computed. A first estimate for the influence of aerosol optical thickness on effective UV indicates an increase in effective UV of 3% for every 0.1 increase in aerosol optical thickness.

Tropospheric ozone
During episode of summer smog the troposphere may contain substantial amount of ozone resulting in a local reduction of the UV dose. We extended the UV mapping procedure to estimate the effect of high tropospheric ozone content. In comparison with direct model computations the effective UV budget derived from this method never deviates more than 0.3%. However, at present we do not have data on tropospheric ozone content with adequate temporal and spatial resolution at our disposal. As a consequence we can not yet visualise the influence of tropospheric ozone on UV budget maps for Europe. A first indication of the magnitude of the effects results in a decrease in effective UV of approximately 4% for every 10 DU increase in tropospheric ozone content

Excess skin cancer risk
Measured local differences in ozone trends will - in combination with a restricted production of ozone depleting substances under the Vienna convention – lead to regional differences in excess skin cancer risk. Preliminary calculations, based on TOMS ozone data, show a variable, but consistent negative ozone trend over Europe for the period 1979-1991. Regional differences over Europe are substantial. The ozone trend (bases on year average ozone concentration) varies from 4% ozone decrease per decade in the central part of north-west Europe (including the Netherlands) to 1% decrease per decade over south Spain and north Scandinavia. Coupling of these trends, after an uncertainty analysis, with the UV chain risk model may in the near future result in regional prognoses for excess risk cancer in 2100.

Cost/benefit of remote sensing
We compared the suitability of remote sensing techniques for UV budget mapping with ground-based UV measurement and with UV model calculations in combination with ozone and cloud measurements from the ground. For the purpose of risk assessments based on UV budget maps, the satellite (TOMS) derived procedure is at present most adequate, mainly because of the long year span of data, spatial coverage, stability an availability of the data. For other purposes however, ground measurement form an indispensable source of additional information.

7.2 Future Research

As concluded above, the RUBEO project is a step forward in the dynamical description of UV budgets in the ongoing efforts to optimise description of surface UV. The improved UV budget mapping is being used in all of RIVM’s environmental assessments, in the National Research Programme on Global Air Pollution and Climate Change (NOP) and in European projects like EDUCE in which RIVM is involved.
To keep the UV mapping state-of-the-art, to further improve the methodology and to improve the applicability, future research and development should focus on the following topics:

1. Full implementation of albedo correction, under clear sky and cloudy conditions, in the UV budget mapping on basis of TOMS minimal reflection data will grade up the accuracy of the UV budget maps. Relating to this topic further data validation is required
2. Exploring for data sets - based on remote sensing or ground measurements – for aerosols and tropospheric ozone with temporal and spatial resolution. Such data sets enable the implementation of aerosol correction and correction for tropospheric ozone, and will further improve the applicability of the UV budget maps.
   The GOME data on stratospheric ozone profiles may yield such a data set for tropospheric ozone.
3. The present UV mapping can work with TOMS and GOME satellite data. So far we used the TOMS data because they provided the longest time series of well defined ozone data. To employ the GOME data set in our environmental and risk assessments it is necessary to make an extensive and long-term comparison of ozone data and UV-budgets derived from assimilated GOME and TOMS data.
4. Additionally, adjustments with respect to the use of satellite reflection data and thorough validation against ground based ozone measurements and UV measurements are needed. The build up of a database with this type of UV data is foreseen in the EC-fifth framework project EDUCE in which RIVM participates.
5. Geographically resolved prognosis for future UV levels and excess skin cancer under the various scenario's of the Vienna convention are needed to get more insight in the future effects of ozone depletion on skin cancer for different locations.
   As a second step the effect of global warming on the expected recovery of the ozone layer should be evaluated. Interaction of ozone and climate change may result in higher UV levels for a longer period of time, which may aggravate effects on human health and environment. At present RIVM participates in a preliminary survey of these interactions in the framework of the National Research Programme on Global Air Pollution and Climate Change (NOP), in the project: 'Ozone and climate interaction effects for ultraviolet radiation and risks', evaluating the effect of global warming on ozone recovery and UV levels over Europe.
   The maps for future risks and other environmental effects are useful in developing and implementing (global) environmental policies counteracting ozone depletion and climate change.
6. To further improve the input data for the UV budget mapping it is necessary to keep in touch with development in remote sensing techniques. In the coming years the Ozone Monitoring Instrument (OMI), may start to produce ozone data with a unique spatial resolution, which can substantially improve the UV budget maps.

Acknowledgements

This study was financially supported by the Netherlands Remote Sensing Board (BCRS) within the framework of the RUBEO project. The methodology for the description of variability in aerosol and tropospheric ozone was derived from the SULPHATE project also supported by the BCRS. The ISCCP-D1 data were obtained from NASA Langley Research Center EOSDIS Distributed Active Archive Center. The global solar irradiance data were obtained from the World Radiation Data Center (WRDC) and the total column ozone data and cloud reflection data from NASA's Nimbus 7 TOMS database.
We thank dr. J. Matthijsen for his contribution to the cloud parameterisation, and we thank dr. P. C. Görts for his review of the manuscript.

References

Bodeker, G.E., Mckenzie, R.L. An algorithm for inferring surface uv irradiance including cloud effects, 1996. J. Appl. Meteorol.. 35 (10):1860-1877.

Bordewijk, J.A., Van der Woerd, H.J., 1997. Ultraviolet dose maps of Europe: A remotesensing/GIS application public health and environmental studies. NUSP-1 report 96-30, RIVM rep. No. 724001004, the Netherlands Remote Sensing Board, Delft.

Borkowski, J.L. 2000 Homogenization of the Belsk UV-B series (1976-1997) and trend analysis. Journal-of-geophysical-research-atmospheres. 2000, 105 (D4):4873-4878 0747-7309.

De Gruijl, F.R. and Van der Leun, J.C. 1995 Estimates of the wavelength dependence of ultraviolet carcinogenesis in humans and its relevance to the risk assessments of stratospheric ozone depletion. Health Phys, 67, 319-325 (1994)

Eck, T. F., P K. Bhartia, Hwang, P.H. and Stowe, L.L. 1987. Reflectivity of Earth's surface and clouds in ultraviolet from satellite observations, J. Geophys. Res., 92, 4287-4296, 1987

Eck, T. F., P K. Bhartia, and J. B. Kerr, 1995. Satellite Estimation of spectral UVB irradiance using TOMS derived ozone and reflectivity, Geophys. Res. Lett., 22, 611-614.

Herman, J., Bhartia, P.K., Ziemke, J., Ahmad, Z., and Larko, D., 1996. UV-B radiation increases (1979-1992) from decreases in total ozone. Geophys. Res. Lett., 23, 2117-2120.

Herman, J.R. and E.A. Celarier, Earth surface reflectivity climatology at 340-380 nm from TOMS data, J. Geophys. Res., 102(D23), 28,003-28,011 (1997).

Herman, J., Krotkov, N.A., Celarier, E., Larko D and Labow, G., 1999 Distribution of UV radiation at the earth's surface from TOMS-measured UV-backscattered radiances. J. Geophys. Res., 104, 12059-12076, 1999

Kalliskota, S.,Kaurola, J., Taalas, P., Herman, J., Celarier, E. and Krotokov, N.A., 2000 Comparison of daily UV doses estimated from Nimbus-7/TOMS measurements and ground-based spectroradiometric data. J. Geophys. Res., 105, 5059-5062, 2000

Krotkov, N.A., Bhartia, P.K., Herman, J., Fioletov, V., and Kerr, J., 1998. Satellite estimation of spectral surface UV irradiance in the presence of tropospheric aerosols, 1, cloud-free case. J. Geophys. Res., 103, 8779-8794.

Levelt, P.F. Allaart, M.A.F., Kelder, H.M., 1996 On the assimilation of total-ozone satellite data. Annales Geophyscae Atmosphere and Space Sciences, November 1996, volume 14 (11) 1111-1118

Madronich, S., 1992. Implications of recent total ozone measurements for biologically active ultraviolet radiation reaching the Earth's surface. Geophys. Res. Lett., 19, 37-40.

Matthijsen, J., Slaper, H., Reinen, H.A.J.M., and Velders, G. J.M., 2000. Reduction of solar UV by clouds: A comparison between satellite-derived effects and ground-based radiation measurements. J. Geophys. Res., 105, 5069-5080, 2000.

McKenzie R., Connor B., Bodeker G., Increased summertime UV radiation in New Zealand in response to ozone loss, 1999, SCIENCE, 285, 1709-1711.

McKinlay, A. and Diffey, B.L., 1987. A reference action spectrum for ultra-violet induced erythema in human skin. in., eds.international congress series. In W.F. Passchier and B.F.M. Bosnjakovich, editors, Human Exposure to Ultraviolet Radiation: Risks and Regulations, pages 83-87. International Congress Series, Elsevier, Amsterdam.

McPeters, R.D., Bhartia, P.K., Krueger, A.J., and Herman, J.R., 1996. Nimbus-7 total ozone mapping spectrometer (TOMS) data products user's guide. NASA/GSFC, Reference Publication, Greenbelt, MD.

Meerkoetter, R., Wissinger, B., and Seckmeyer, G., 1997. Surface UV from ERS-2/GOME and NOAA/AVHRR data: A case study. Geophys. Res. Lett., 24, 1939-1942.

NSTC, 1999 Our changing planet A report by the subcommittee on global change research, committee on the environment and natural resources of the National Science and technology council. A supplement to the President’s fiscal year 1999 budget

Outer, P.N. 1999, UVTRANS model beschrijving, RIVM, internal document.

Outer, den P.N., Slaper, H.,Matthijsen, J., Reinen, H. A. J. M. and Tax, R. 1999 Variability of ground level ultraviolet: model and measurement. Proceedings of an international workshop, published in: Radiation Protection Dosimetry, vol. 91, Nrs 1-3, pp105-110 (2000), Nuclear Technology Publishing

Rossow, W.B., Schiffer, R.A. 1991 ISCCP cloud data products bulletin of the American Metorological Society, Vol.72, no 1, 2-20,1991

Rossow, W.B., Walker, A.W. and Garder, L.C. 1993 Comparison of ISCCP and other cloud amounts, J. Clim., 6, 2394-2418, 1993

Rossow, W. B., Walker, A.W.,Beuschel, D.E. and Roiter, M.D. 1996 International satellite cloud climatology project (ISCCP): Documentation of new cloud data sets,WMO/TD-737, 115 pp., World Metereol. Organ., Geneva

Slaper, H., 1987 PhD thesis Utrecht University

Slaper, H., Daniel, J.S., de Gruijl, F.R., and van der Leun, J.C., 1996. Estimates of ozone depletion and skin cancer incidence to examine the Vienna convention achievements. NATURE, 384, 256-258.

Slaper, H., Velders, G. J.M., and Matthijsen, J., 1998. Ozone depletion and skin cancer incidence: a source risk approach. J. Hazardous Mat., 61, 77-84.

Slaper, H., Matthijsen, J.,den Outer, P.N., Velders, G. J.M., 2001 Climatology of Ultraviolet Budgets using Earth Observation (CUBEO): mapping UV from the perspective of risk assessments. Report by Beleidscommissie remote sensing (BCRS), User Support program, USP-2 00-17, ISBN 90 54 11 32 6

Spinhirne, J.D. and Green, A.E.S. 1978 Calculations of the relative influence of cloud layers on received ultraviolet and integrated solar radiation, Atmos. Environ.,12, 2449-2454, 1978

UNEP, 1998. Environmental Effects of Ozone Depletion: 1998 Assessment. Photochem. Photobiol. B.: Biology, 46, 1-108.

Verdebout, J. A method to generate surface uv radiation maps over europe using gome, meteosat, and ancillary geophysical data. 2000 J. Geophy. Res Atmosp. 105(D4), 5049-5058. 2000.

Weele, M. van, T. J. Martin, M. Blumthaler, C. Brogniez, P. N. den Outer, O. Engelsen , J. Lenoble, G. Pfister , A. Ruggaber, B. Walravens, P. Weihs, H. Dieter, B.G. Gardiner, D. Gillotay, A. Kylling, B. Mayer, G. Seckmeyer, W. Wauben, 2000. From model intercomparison towards benchmark UV spectra for six real atmospheric cases, J.Geophys. Res., 105, 4915-4925.

Weatherhead, E.C., Tiao, G.C., Reinsel, G.C., Frederick, J.E., Deluisi, J.J., Choi, D.S., Tam, W.K, 1997. Analysis of long-term behavior of ultraviolet radiation measured by robertson-berger meters at 14 sites in the united states. Journal-of-geophysical-research-atmospheres. 102 (D7):8737-8754

WMO, 1995. Scientific Assessment of Ozone Depletion: 1994, Global Ozone Research and Monitoring Project. WMO/Rep. Nr. 37, Geneva.

WMO, 1999. Scientific Assessment of Ozone Depletion: 1998, Global Ozone Research and Monitoring Project. WMO/Rep. Nr. 44, Geneva.

World Meteorological Organisation (WMO), 1978 Input format guidelines for world radiometric network data,WMO/TD-253, St. Petersburg, Russia, 1987

Zerefos C., Meleti C., Balis D., Tourpali K., Bais A.F., 1998 Quasi biennial and long-term changes in clear sky UV-B solar irradiance, Geophys. Res. Lett., 25, 4345-4348.

Appendix A: List of Acronyms

AMOUR	- Assessment MOdel for Uv Radiation and Risks, (pre-operational) model under development in the context of CUBEO and RUBEO projects from BCRS.
BCC	- Basal Cell Carcinoma
BCRS	- BeleidsCommissie voor Remote Sensing, the Netherlands Remote Sensing Board
CA	- Copenhagen Amendment. A reduction scenario (under the Vienna convention) resulting in zero production of ozone depleting substances at the end of 1995.
CIE	- Commision Internationale de l'Ėclairage
CMM	- Cutaneous Malignant Melanoma
CUBEO	- Climatology of Ultraviolet radiation Budgets using Earth Observation, project at RIVM financially supported by the BCRS
CUVRA	- Characteristics of UV-radiation in the Alps; fourth framework EU-project
DU	- Dobson Unit, unit for ozone column thickness. An ozone column of 300 DU corresponds at standard pressure (1 atmosphere) and temperature (0˚C) to a layer of ozone of 3 mm thickness.
EDUCE	- European Database for Ultraviolet radiation Climatology and Evaluation; fifth framework EU-project; follow up of the SUVDAMA project
EEA	- European Environmental Agency
ESA	- European Space Agency
EU	- European Union
FMI	- Finnish Meteorological Institute
GDF	- Ground Derived UV-reduction Factor for the evaluation of cloud effects on ground level UV, using an empirical relationship based on ground-based pyranometer data
GOME	- Global Ozone Monitoring Experiment on board ESA's ERS-2 satellite;
IASB	- Institut d'Aeronomie Spatiale de Belgique
ISCCP	- International Satellite Cloud Cover Project
ISCCP-DF	- ISCCP (satellite) derived daily UV reduction factor
IVM	- Instituut Voor Milieuvraagstukken, Vrije Universiteit Amsterdam
KNMI	- Koninklijk Nederlands Meteorologisch Instituut
KMI	- Koninklijk Meteorologisch Instituut voor België
LIDAR	- Light Detection and Ranging. Instrument measuring ozone concentration in the atmosphere by detecting backscattering from pulsed light.
MAUVE	- Mapping UV by Europe, EU-project within the fourth framework program
MLS	- Mid Latitude Standard atmosphere
MP	- Montreal protocol. A reduction scenario (under the Vienna convention) resulting in a reduction of 50% in the production of ozone depleting substances at the end of 1999
NASA	- National Aeronautics and Space Administration
NIVR	- Nederlands instituut voor Vliegtuigontwikkeling en Ruimtevaart, Netherlands Agency for Aerospace Programs
NOP	- Nationaal Onderzoeksprogramma, Dutch National Research Programme on Global Air Pollution and Climate Change

NR	- No Restriction scenario. A scenario (under the Vienna convention) assuming a yearly rise in the production of ozone depleting substances of 3% per year
nm	- nanometer, 1 nm $=10^{-9}$ meter
OMI	- Ozone Monitoring Instrument
RB	- Robertson Berger UV-biometer, instrument applied at RIVM to measure erythemally weighted UV-irradiances
RIVM	- Rijks Instituut voor Volksgezondheid en Milieu, National Institute of Public Health and the Environment
RUBEO	- Risks and Ultraviolet Budgets using Earth Observation, project at RIVM financially supported by the BCRS
SCC	- Squamous Cell Carcinoma
SCUPh	- Skin Cancer action spectrum developed at the Skin and Cancer Hospital in Philadelphia and the University of Utrecht. The h denotes a correction on the action spectrum originally developed in mice, for transmission through human epidermis.
SULPHATE	- Surface Ultraviolet Levels; Prediction and History from Atmospheric Trends over Europe
SUVDAMA	- Scientific UV DAta Management, EU-project within the fourth framework program; spectral UV-measurements are used from the European UV-database designed within this project
SZA	- Solar Zenith Angle
TOMS	- Total Ozone Monitoring System, on board of NIMBUS 7, METEOR and Earth Probe satellites; source for total ozone measurements
TOMS-DF	- TOMS (satellite) derived daily UV reduction factor
UNEP	- United Nations Environmental Program
USP	- User Support Program, a program under responsibility of BCRS
UV	- Ultraviolet radiation (wavelength range 100-400 nm)
UVA	- Ultraviolet radiation in the wavelength range 315-400 nm
UVB	- Ultraviolet radiation in the wavelength range 280-315 nm
UVC	- Ultraviolet radiation in the wavelength range 100-280 nm
UVTRANS	- Two stream atmospheric UV-transfer model developed at RIVM
VROM	- Ministerie van Volkshuisvesting Ruimtelijke Ordening en Milieu; Dutch Ministry of Housing, Physical Planning an the Environment
WMO	- World Meteorological Organisation
WRDC	- World Radiation Data Center, data center from which the global radiation measurements were obtained